JOURNAL OF PROPULSION AND POWER
Vol. 24, No. 5, September–October 2008

Virtual Shapes in Supersonic Flow Control with Energy Addition

M. N. Shneider,* S. O. Macheret,† S. H. Zaidi,‡ I. G. Girgis,§ and R. B. Miles¶
Princeton University, Princeton, New Jersey 08544

DOI: 10.2514/1.34136

This paper presents a short selective review of theoretical and experimental studies conducted by the authors and their collaborators during the past few years in areas related to supersonic and hypersonic flow regimes with applications such as drug reduction, inlet and effective vehicle geometry control in off-design flight regimes, and steering and sonic boom mitigation. Their results suggest a principal possibility to enable transitions between the propulsion modes and ramjet startup and to minimize the need for the traditional isolator stage, as well as to increase the inlet mass capture at Mach numbers below the design value, using active control based on virtual shapes created by energy addition upstream of the inlet throat. A common feature of all these substantially different applications and processes is a power deposition into a supersonic flow which results in the creating of virtual shapes, modifying flowlike solid obstacles immersed in it. The virtual shapes can be created by microwave plasma heating, magnetohydrodynamic forces, electron beams, and localized plasma-assisted surface combustion. The power necessary to operate plasmas can come either from the turbine at mode transition, from an auxiliary power unit, or, as suggested in a new bypass concept, from a magnetohydrodynamic generator either placed downstream of the combustor or collocated with it.

I. Introduction

ENERGY addition for modification of the external flowfield around a vehicle is a very well-known technique and, primarily, has been studied and used to reduce the drag on the objects flying at supersonic speeds. Historically, energy addition in the supersonic flow was proposed as an alternative technique of reducing drag on a flying object [1–3].

Studies of supersonic gas flows with energy input organized in one way or another are of considerable interest. Given an appropriate position, shape, and power of the thermal source relative to the external surface of the body, one can substantially decrease its aerodynamic drag and thereby reduce the value of thrust required to maintain the steady flight. Such reasoning was discussed in a number of papers [1–13]. The problem of supersonic flow past a localized region of heat release was treated by many researchers around the world [4–13].

In addition to drag reduction, other applications of energy addition to external high-speed flows have been suggested recently. Those include, for example, control of oblique shock waves and optimization of scramjet inlets, control of shock reflection and boundary-layer separation, and sonic boom mitigation. This paper is not intended as a comprehensive review of the area. Rather, we consider results of aerodynamic flow control by energy deposition obtained by the Princeton group and their collaborators during the past few years, and to some extent reflected in the state-of-the-art reviews on this topic. The principal topics of the present review include: 1) The effect of a plasma (directed-energy) air spike in supersonic/hypersonic flows. The similarity laws for shock wave and drag parameters, as functions of the strength of heat source and characteristics of incident flow, and experimental and computational parametric studies; 2) modeling of "virtual cowl," that is, of energy addition to hypersonic flow off the vehicle to increase air mass capture and reduce spillage in scramjet inlets at Mach numbers below the design value; 3) shortening the isolator by heat addition upstream of the inlet throat; 4) new bypass concept: power for virtual cowl and/or plasma regions in the isolator: from the magnetohydrodynamic (MHD) generator inside or behind the combustor; 5) numerical studies of aerodynamic forces created by off-axis heat addition upstream of a body with possible applications in supersonic/hypersonic vehicle steering; 6) experiments and numerical modeling of pulsed off-body energy addition for sonic boom mitigation.

II. Supersonic Flow with Concentrated Stationary Energy Source in Front of Body

The possibility of reducing the drag of a body moving in the atmosphere at a supersonic speed by releasing the energy upstream of the body has been discussed and studied for almost half a century [1,2]. The force acting on the body on the side of incident flow (in a system of coordinates with the body at rest) decreases because of deflection of a part of the flow incident on this body, thereby decreasing the pressure on the body. The flow deflects as a result of refraction of a shock wave on a curvilinear surface; this shock wave propagates from the point of energy release as if from a point of explosion. The effect of energy release was demonstrated experimentally. To reduce the supersonic drag of a blunt body, a metal spike is sometimes provided on its nose. Such a telescopic spike was mounted on the U.S. Trident-3 rocket. The burning of hydrogen delivered to the spike end caused a 50% drag reduction compared with experiments without burning and a 75% reduction compared with experiments without a spike [3]. Recently, a number of numerical calculations have been performed on supersonic flow past the region of energy release [4], on flow past bodies of different shapes in the presence of a source of energy preceding these bodies, and on drag reduction [8–13]. Experiments were also performed with laser [14] and microwave pulses and discharges for initiating energy release, as a rule, at low values of Mach number and average power.

Presented as Paper 3862 at the 34th AIAA Plasmadynamics and Lasers Conference, Orlando, FL, 23–26 June 2003; received 19 August 2007; accepted for publication 12 March 2008.

*Research Scientist, Department of Mechanical and Aerospace Engineering, D-414 Engineering Quadrangle; shneyder@princeton.edu. Senior Member AIAA.

†D-414 Engineering Quadrangle; currently Senior Staff Aeronautical Engineer, Lockheed Martin Skunk Works, 1011 Lockheed Way, Palmdale, California 93599-0160; sergey.macheret@lmco.com. Associate Fellow AIAA.

‡Research Scientist, Department of Mechanical and Aerospace Engineering, D-414 Engineering Quadrangle. Member AIAA.

§Research Associate, Department of Mechanical and Aerospace Engineering, D-414 Engineering Quadrangle; currently Principal Scientist, Johnson & Johnson Pharmaceutical Research and Development; igirgis@prdus.jnj.com. Associate Fellow AIAA.

¶Professor, Department of Mechanical and Aerospace Engineering, D-414 Engineering Quadrangle. Fellow AIAA.

Recent reviews [15,16] are devoted to this problem. Studies of an "air spike" with plasma power deposition into hypersonic flow were initiated by Myrabo and Raizer [17]. They suggested that a focused laser beam can be used to deliver power in front of a projected vehicle. They revealed the effect of drag reduction owing to energy release, whereby an appreciable amount of energy could be saved. To demonstrate this effect, Myrabo et al. conducted an experiment involving the use of an electric arc as the source of energy [18]. In recent papers [19,20], both the air-spike experiment and theory have been basically improved compared to the earlier work [6,17], as far as the electrode's design and configuration to produce the arc in the flow is concerned.

A. Freestream Hypersonic Flow with Localized Power Deposition

The approximate analytical theory for a shock created in a supersonic flow by a concentrated energy release with power P can be described as follows. In the reference frame moving with the incident flow, having velocity u_0, the shock wave can be considered as a cylindrical shock wave created by the axial energy input $E_1 = P/u_0$ J/cm. The law of self-similar propagation of a strong blast wave induced by a cylindrical explosion has the form [17]

$$R = \alpha\left(\frac{E_1}{\rho_0}\right)^{\frac{1}{4}} t^{\frac{1}{2}} = \alpha\left(\frac{P}{\rho_0 u_0}\right)^{\frac{1}{4}} t^{\frac{1}{2}} \tag{1}$$

where ρ_0 is the freestream density. The numerical coefficient α can be determined with sufficiently high accuracy using the method proposed in [21]. Because the point R on the shock wave front moves along the z axis with the velocity of incident flow u_0, one can substitute $t = z/u_0$ into Eq. (1). As a result, the equation that describes the shape of axisymmetric shock front in the reference frame that is stationary with respect to the body is

$$R = \alpha\left(\frac{P}{\rho_0 u_0^3}\right)^{\frac{1}{4}} z^{\frac{1}{2}} = \alpha b^{\frac{1}{2}} z^{\frac{1}{2}}, \qquad b = \left(\frac{P}{\rho_0 u_0^3}\right)^{\frac{1}{2}} \tag{2}$$

Thus, the shock wave front has a parabolic shape $z \sim R^2$, satisfying the simple similarity law that follows from Eq. (2) [17]:

$$R/b = \alpha(z/b)^{1/2} \tag{3}$$

The fraction of incident flow that is deflected and does not hit the body characterizes the decrease in aerodynamic drag. The approximate similarity laws for the shape and parameters of the strong shock wave as functions of the strength of heat source and characteristics of freestream flow, which enable one to make scaling predictions, were obtained in [19]. Assuming that the shock is strong and disregarding the static pressure of the freestream, the scaling laws are

$$\frac{R}{b} = \varphi\left(\frac{z}{b}\right), \qquad p_f = \rho_0 u_0^2 f\left(\frac{z}{b}\right), \qquad f = \frac{2\varphi'^2}{(\gamma+1)(1+\varphi'^2)} \tag{4}$$

where p_f is the pressure behind the shock wave front. Here, the function φ characterizes the shape of the shock wave (SW) surface on which the supersonic flow is refracted, and the function f is determined by the slope of incident flow with respect to the normal to the SW surface at a given point. The scaling relations in Eq. (4) can be used with function φ that was either experimentally measured or calculated by numerous simulations. The scaling laws in Eq. (4) permit us to derive the SW parameters for other conditions of supersonic/hypersonic flow and for other values of power for a stationary heat source, without performing laborious experiments or numerical calculations for each specific case. In particular, the results of calculations for Rensselaer Polytechnic Institute (RPI) Hypersonic Shock Tunnel (HST) experimental conditions (Mach number of the incident flow $M = 10.1$, static pressure $p_0 = 5.6 \times 10^{-3}$ psi $= 38.6$ Pa, static temperature $T_0 = 37.7$ K) are in good agreement with the approximate formulas [Eqs. (1–4)] (Figs. 1–3) [22,23].

The numerical simulations of RPI experiments were performed using a standard Euler routine including equations of continuity, momentum, and energy with energy addition source term [6,19]. The volume heating source term, which in this model is meant to simulate the thermal energy deposited in the flow due to the electric arc, was varied with the goal of finding the power level that results in the experimentally observed shock wave pattern. This power level turned out to be around 15 kW.

The results of numerical simulation for 15 kW heat source power are given in Figs. 2 and 3, where the flow streamlines and contours of pressure and density are shown. Figure 4 shows a comparison of experimental schlieren images, with the density plots also separately shown in Fig. 3. A 64 kW energy source was used in the schlieren experiment and it was assumed that only 15% of this energy was directly coupled to the flow as heat. One can see that a parabolic shock wave is formed, and that the gas behind the shock wave is strongly rarefied and heated. The incident streamlines are refracted by the shock wave, and the effects of heating on the flowfield can drastically change the drag on a body in the flow.

B. Modification of Effective Body Shape by Energy Addition in Front of Body

Recent RPI experiments show the principal possibility of changing the effective geometry of a blunt body by energy addition in hypersonic flow, resulting in a substantial reduction in drag [22–24]. The results presented in Figs. 5–7 show very clearly how the oblique shock wave deflects the streamlines far upstream of the body, and how the pressure at the body surface is decreased in comparison with the case of no energy addition. Without energy addition, the

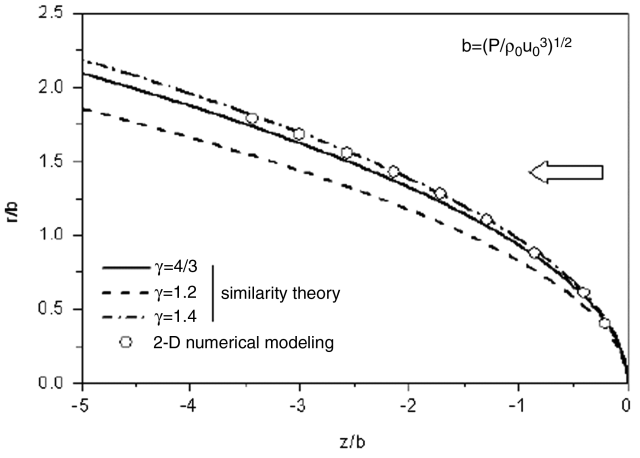

Fig. 1 Shape of shock wave surface in relative units corresponding to similarity laws, Eqs. (3) and (4), at different γ, and results of 2-D numerical modeling.

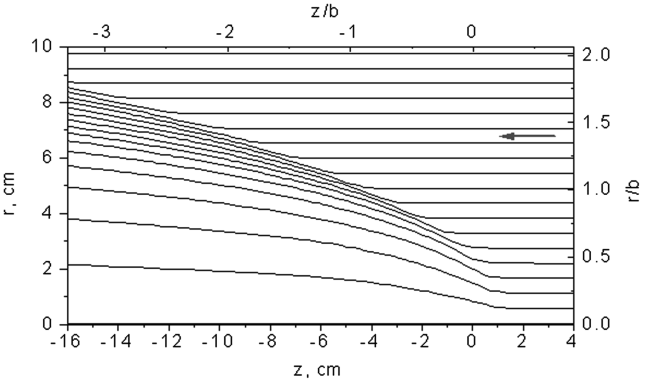

Fig. 2 Streamlines for shock wave shown in Fig. 1. Heat source of $P = 15$ kW is located at $z = 0$. Flowfield is universal in dimensionless variables corresponding to similarity law.

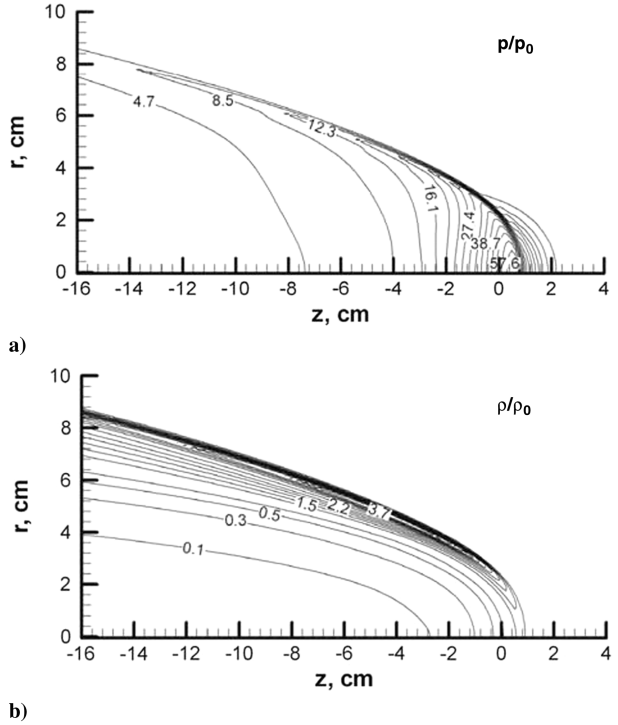

Fig. 3 Pressure and density contour lines. Heat source of $P = 15$ kW is located at $z = 0$. No blunt body is positioned downstream.

computational model predicts that the maximum pressure on the surface of this blunt body is about 120 p_0, and the bow shock is located 2.3 cm upstream of the body, in close agreement with experiments, as shown in Fig. 5.

Using the results of numerical calculations, it is possible to find the integral of pressure along the body surface that is the drag force

$$F = \oint_S p_s \cos\alpha \cdot 2\pi(r/\cos\alpha)\,\mathrm{d}r = 2\pi \int_0^a p_s r\,\mathrm{d}r \qquad (5)$$

When this is done, the drag force is found to be 13.5 N compared with 48.3 N when the heat source is moved closer to the body ($L = 0.6$ D), and 70.33 N when there is no heat source. If this body were flying through the atmosphere, then to maintain the flight speed u_0 corresponding to the energy addition experiment, the total propulsive power expended would need to be 21 kW, according to $P_{\text{total}} = Fu_0 + P$, where P is the power added to the flow by volume heating. For the case when $L = 0.6$ D, the corresponding value of propulsive power is 55.8 kW, and when there is no energy addition, $P = 0$, it is 84.1 kW.

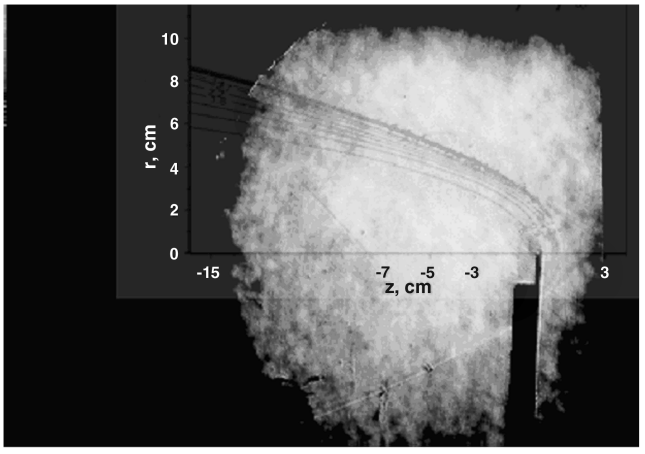

Fig. 4 Schlieren image of flow with 62 kW overlaid with calculated density plot from Fig. 3 (15 kW) [19].

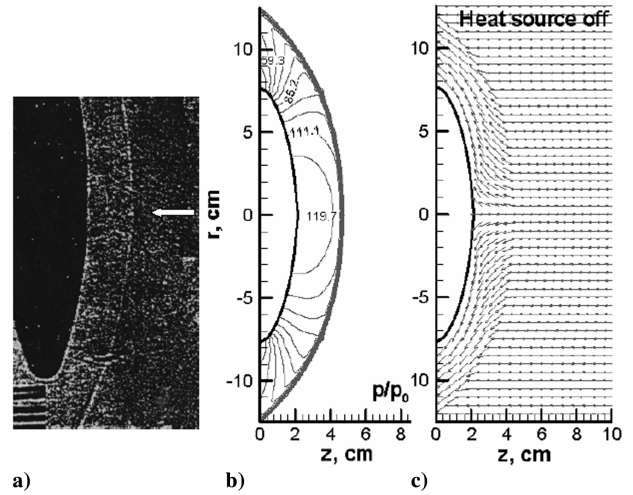

Fig. 5 Bow shock wave in case of no heat addition in flow: a) experiment [23,24], b–c) numerical modeling: b) isobars, c) streamlines.

Unlike in the case with energy addition to a freestream flow without the blunt body (Figs. 3 and 4), the shock wave in Fig. 6 is conical. However, when the heating source is moved farther from the body, as L increases, the shock wave becomes parabolic again [24] (Fig. 7) and the standoff distance increases drastically due to substantial decrease of the Mach number behind the heat source.

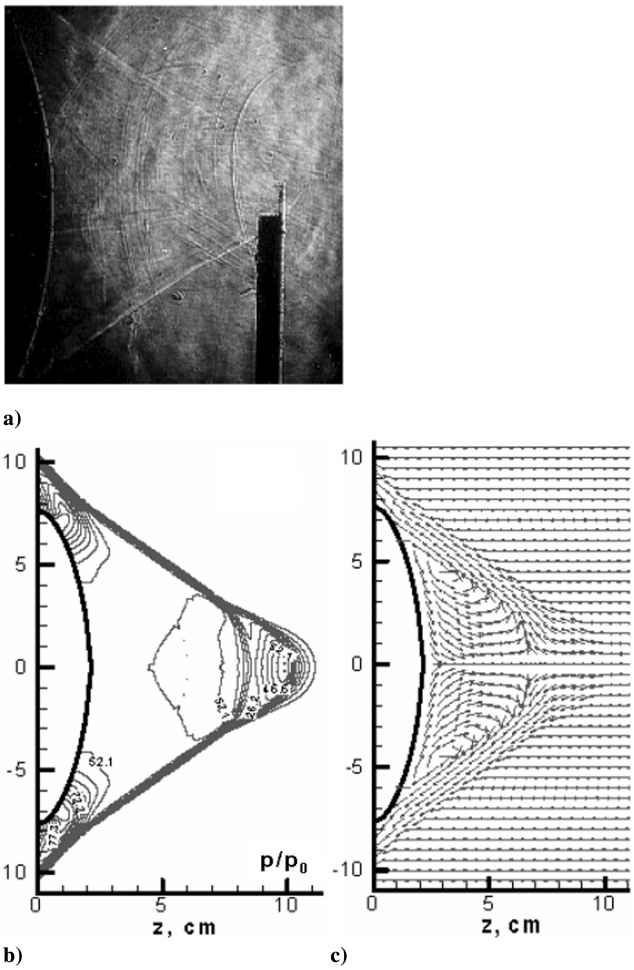

Fig. 6 Schlieren image of Mach 10, 27 kW arc [23,24] (arc-body separation is 60% of blunt body diameter); Computed shock wave structure (isobars) and flow streamlines at $P = 7.5$ kW, $L = 0.6$ D.

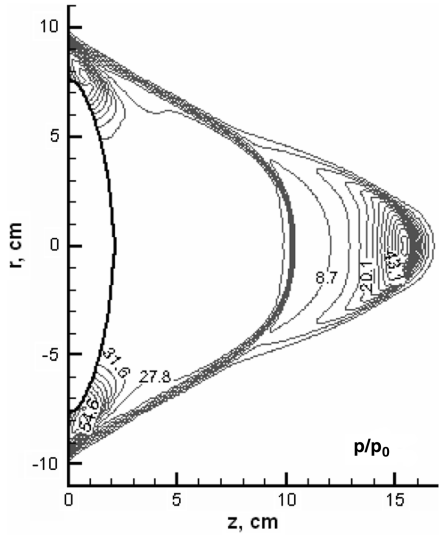

Fig. 7 Computed isobars at $P = 7.5$ kW and $L = D$.

To create a parabolic SW and to substantially reduce the drag, a localized intense power deposition on the order of $P \sim P_D = 0.5\rho_\infty u_\infty^3 A$, where A is the blunt body cross-sectional area, is required. Note that this power is comparable with the drag power. An alternative approach was suggested recently by Kolesnichenko et al. [25,26] and studied experimentally and theoretically. The results of this investigation show that a very long, needlelike heat source in front of the blunt body causes bow shock wave reorganization with substantial drag reduction, even with a relatively low heating power. Similar results were obtained by Georgievsky and Levin in recent numerical modeling for spheres and cones in supersonic flow [27]. This approach looks very interesting and promising, because of the very low power consumption as compared with localized directed-energy air spike, and it needs to be carefully studied.

III. Plasma Virtual Shapes in Hypersonic Propulsion Flowpath

The development of viable hypersonic airbreathing combined-cycle cruise and space launch vehicles faces a number of technical challenges [28]. Some of these challenges stem from the need to operate in a wide range of Mach numbers. For example, as the vehicle passes through approximately Mach 3.5–4, the engine needs to change from turbine operation to ramjet operation. This process will likely involve a change in the flowpath and requires a guaranteed starting mechanism for the ramjet engine to assure that the transition occurs smoothly. Normally, that starting mechanism involves reducing the contraction ratio by opening up the inlet, isolator, and engine flowpath cross-sectional area or rotating the cowl leading edge to reduce the air capture ratio [29]. The contraction ratio is then increased by reducing the area or rotating the cowl leading edge to improve the compression and produce acceptable engine performance. It is worth mentioning that, conventionally, the changes in contraction ratio are produced by a complex, heavy, and slow-reacting electrohydraulic system.

The ramjet engine needs to operate with subsonic or transonic air entering the combustor. Typically, this is achieved with a long isolator stage, which acts as a supersonic diffuser to slow the inlet flow to subsonic Mach numbers [29]. Under high-speed operation, there are no strong shocks in the isolator, just a weak oblique shock system downstream of the throat. This results in small inlet losses and a clean profile at entry to the combustor, but it requires significant length to keep the adverse pressure gradients small and avoid separation. Furthermore, it is necessary to ensure that the terminal shock does not move upstream of the throat because the shock position is unstable under these conditions and the engine will unstart. Normally, strong suction is used to control the shock position and avoid unstart, adding to the overall weight and complexity of the engine.

The ramjet is only used to accelerate the vehicle up to about Mach 5 or 6, at which point the scramjet takes over. Cruise conditions are hypersonic: there is no "design" condition for the ramjet because it is only a transitional stage. Consequently, 1) some level of performance loss can be tolerated during the transient ramjet operation, 2) a long isolator stage adds considerable weight to the engine, and 3) the isolator interior is a major part of the cooling load, particularly at high Mach number when the isolator is still in the flowpath, but not needed. In recent papers [30–32], we proposed the use of heat addition upstream of the inlet throat to reduce the Mach number and thus substantially shorten or even eliminate the isolator. Although a substantial amount of power would be needed for this heat addition, and stagnation pressure would be reduced, the thrust penalty in the acceleration stage can be offset by the increased performance during the hypersonic cruise, stemming from the shortening or elimination of the isolator.

Another group of challenges is associated with the need to optimize the inlet geometry. The optimum geometry corresponds to the well-known shock-on-lip (SOL) condition: the compression ramp shocks converge on the cowl lip (CL), and the reflected shock impinges on the upper boundary of the inlet [28]. Because shock angles are determined by the flight Mach number, the SOL condition cannot be met at Mach numbers higher or lower than the design Mach number [28]. At Mach numbers higher than the design value, the shocks move inside the inlet, causing multiple reflected shocks, loss of stagnation pressure, possible boundary-layer separation, and engine unstart. At Mach numbers lower than the design value, a portion of the air compressed by the shock misses the inlet ("spillage"), and the air mass capture decreases.

At off-design Mach numbers, energy addition to or extraction from the flow, using plasmas and various magnetohydrodynamic devices, can be considered as an alternative to a variable geometry inlet. An important advantage of plasma-based methods of inlet and isolator control is their flexibility, controllability, and fast response.

At Mach numbers higher than the design value, it can be possible to move the shocks from inside the inlet back to the cowl lip by an MHD generator device placed at one of the compression ramps. This method, while providing some flexibility of flow control, would not require any net power to run the MHD device, because the generator mode would be used, and the power requirements for air ionization can be minimized with electron beams as ionizers [33–44]. Principal disadvantages of the method include stagnation pressure losses due to the inevitable joule heating, and also the weight of the magnet and other hardware.

In our papers [33–35,37–44], we demonstrated that this approach to MHD inlet control can yield an acceptable inlet performance while operating in the mode of net power extraction. We showed that the MHD region should be quite short (typically 25–30 cm along the flow) and be located as far upstream as possible [33,35].

To increase air mass capture and reduce spillage in scramjet inlets at Mach numbers below the design value, we have suggested the use of energy addition to the flow off the vehicle. The heated region would create a "virtual cowl" that would deflect the flow streamlines into the inlet [45,46]. Various mechanisms of energy addition can be used. For example, the heated region may be generated by supplying microwave or RF energy to a volume preionized by a focused laser or electron beam. Other possible means include plasma or hot-air jets, and external combustion. An important advantage of the new method is that the air entering the inlet would have experienced little or no heating [47–49]. Thus, irreversibilities and stagnation pressure losses associated with heating can be minimized. Optimization studies showed that the best location of the energy addition region is near the intersection of the nose shock of the vehicle with the continuation of the cowl line, and slightly below that line [48].

A. Virtual Cowl: Concept and Applications

The virtual cowl concept involves energy addition to hypersonic flow off the vehicle to increase air mass capture and reduce spillage in scramjet inlets at Mach numbers below the design value.

The optimum geometry of scramjet-powered hypersonic vehicles corresponds to the well-known shock-on-lip condition (Fig. 8): the compression ramp shocks converge on the cowl lip, and the reflected shock impinges on the shoulder of the inlet [23]. Because shock angles are determined by the flight Mach number, the SOL condition cannot be met at Mach numbers higher or lower than the design Mach number [23]. Typically, inlets are designed for the highest Mach number expected in the hypersonic airbreathing flight, and at Mach numbers lower than the design value, the so-called spillage occurs, and the air mass capture decreases (Fig. 9).

To reduce the spillage, the cowl might be extended upstream, although this could be difficult to accomplish practically. However, the case with extended solid cowl can serve as a guide to optimizing virtual cowl cases. Qualitatively, one would expect that the virtual cowl (i.e., off-body energy addition) should, for the best performance, create a flow pattern imitating that of the solid extended cowl. Because shocks do not reflect off a heated region, the analogy between the solid and virtual cowls is not exact. However, the heated region can generate a shock wave that would mimic the shock reflected from the solid surface upon incidence of the nose shock on it. Thus, one would expect that the energy addition should be more or less concentrated, and that it should be positioned near the intersection of the nose shock with the upstream continuation of the cowl. Note that heating and the resulting expansion of the gas would adversely affect both mass flow rate and stagnation pressure at the throat if the heated air is allowed to enter the inlet. Therefore, the energy addition region should be shifted somewhat down, so that heated and expanded air would miss the inlet, while cold air would be compressed and deflected into the inlet.

In recent papers [31–35,45–47], we analyzed a new concept of increasing the mass capture, suggested in [45], and named a virtual cowl. The essence of the method is to create a heated region upstream of and somewhat below the cowl lip (Fig. 10). The incoming flow would be deflected by the elevated-temperature and/or elevated-pressure region, causing an increased mass flow into the inlet (in some sense, the air deflection by the virtual cowl is analogous to an air-spike effect, considered in the previous section). The mechanism of energy addition was unspecified. For example, the heated region may be generated by supplying microwave or RF energy to a volume preionized by a focused laser or electron beam. Other possible means include plasma or hot-air jets, and external combustion. An important advantage of the new method is that the air entering the inlet would have experienced little or no heating. Thus, irreversibilities and stagnation pressure losses associated with heating can be minimized.

In [45,46], the virtual cowl concept was computationally studied, and the optimum location and shape of the heat addition region was determined, without specifying the energy addition mechanism.

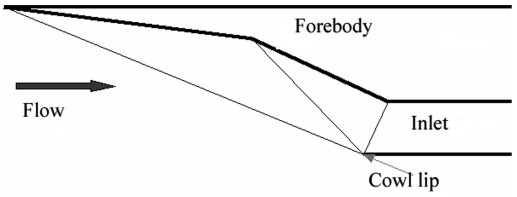

Fig. 8 Design forebody and inlet geometry with shock-on-lip condition.

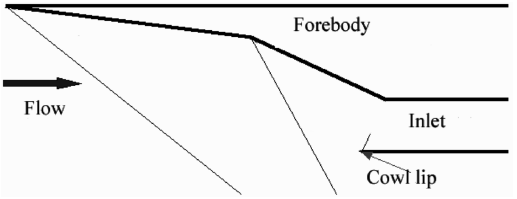

Fig. 9 Flow and shock geometry at Mach number lower than design value, with no plasma or MHD control.

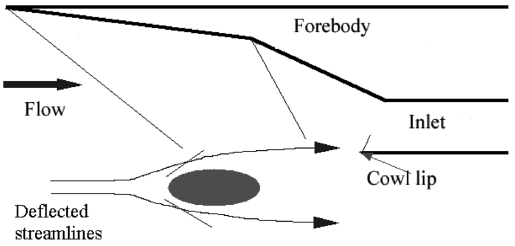

Fig. 10 Schematic diagram of virtual cowl concept: off-body heat addition increases mass capture.

1. *Model and Computational Procedure*

We consider hypersonic gas flow along a series of compression ramps upstream of the inlet with forward-shifted cowl lip, as schematically shown in Fig. 10. The flow is two-dimensional in the (x, z) plane. Cases both without and with heat addition are computed with the set of Euler equations together with the perfect gas equation of state. Because the entire flow region is supersonic, a steady-state solution using x as a marching coordinate can be found. The heat addition rate profile is Gaussian, that is, it is proportional to $\exp[-(x-x_0)^2/r_{\text{eff},x}^2 - (z-z_0)^2/r_{\text{eff},z}^2]$, where x_0 and z_0 are coordinates of the center of the heating region, and $r_{\text{eff},x}$ and $r_{\text{eff},z}$ are the effective radii. The parameters x_0, z_0, $r_{\text{eff},x}$, and $r_{\text{eff},z}$ are varied in computations to find optimal values of these parameters. In "circular-cylinder Gaussian" cases, $r_{\text{eff},x} = r_{\text{eff},z} = r_{\text{eff}}$. In "elliptical-cylinder Gaussian" cases, $r_{\text{eff},x} \neq r_{\text{eff},z}$, the heating profile may also be tilted at an angle α_q with respect to the x axis.

The inlet performance is characterized by the total enthalpy entering the inlet throat per second per unit length in the spanwise direction $\dot{H}$, the average Mach number at the throat M, the mass capture coefficient k_m, the ratios of stagnation pressure and static pressure, density, and temperature at the throat to their freestream values (k_{p_t}, k_p, k_ρ, and k_T), and adiabatic and cooled kinetic energy efficiencies, $\eta_{\text{KE,ad}}$ and $\eta_{\text{KE,cool}}$.

In many cases, the flow at the inlet throat is quite nonuniform and not parallel to the walls. Therefore, a proper procedure of averaging flow parameters at the throat has to be employed. In this work, we use the so-called stream-thrust averaging commonly accepted in inlet design [29]. This procedure, described in [29], effectively takes into account losses of total pressure (entropy increase) that would occur downstream of the throat, in the isolator, when the flow is allowed to settle and to become parallel to the walls.

The modeling performed in [31,32,35–46] demonstrated that a virtual cowl created by energy deposition upstream of the cowl lip can substantially increase mass capture and kinetic energy efficiency of the inlet. The performance of virtual cowl can approach or match that of a would-be upstream solid extension of the cowl. With the power deposition of only 2–3.5% of the enthalpy flux into the inlet, the mass flow rate entering the inlet and the compression ratio can be increased each by 15–20% (at Mach 6), with no loss of kinetic energy efficiency. Note that, recently, a combination of the virtual cowl concept with MHD inlet control and energy bypass was also considered by Kuranov and Sheikin, and their findings are detailed in [47].

2. *Examples of Computed Cases*

Freestream conditions in all computed cases in [46] corresponded to flight at Mach 6, 8, or 10, with dynamic pressure of either 1000 or 2000 psf. The freestream parameters are listed in Table 1. The baseline case was that of Mach 10 flight with 0 deg angle of attack. The three-ramp inlet (2.5, 8.0, and 11.0 deg ramp angles) was chosen so that the nose shock would barely (by about 1 in.) miss the cowl lip, and the flow would be almost parallel to the isolator walls downstream of the inlet throat. This design geometry, as well as shock patterns at Mach 6 and Mach 8, with flow spillage, are shown in Fig. 11. Figure 12 shows static temperature contours and flow streamlines at Mach 6, 2000 psf, demonstrating the spillage. The arrow in Fig. 12, and in subsequent figures in this paragraph, indicates the position of inlet throat.

Table 1 Freestream parameters: altitude h, static pressure and temperature, p_0 and T_0, in computed cases with flight dynamic pressure of $q = 1000/2000$ psf

Mach	h, km	p_0, Pa	T_0, K
6	26.93/22.47	1900/3800	223.47/218.98
8	30.76/26.155	1068.75/2137.5	227.26/222.70
10	33.789/29.108	684/1368	233.16/225.63

To reduce the spillage, the cowl might be extended upstream, as illustrated in Fig. 13, although this can be difficult to accomplish practically. However, the case with extended solid cowl can serve as a guide to optimizing virtual cowl cases. Qualitatively, one would expect that the virtual cowl (i.e., off-body energy addition) should, for the best performance, create a flow pattern imitating that of the solid extended cowl. Because shocks do not reflect off a heated region, the analogy between the solid and virtual cowls is not exact. However, the heated region can generate a shock wave that would mimic the shock reflected from the solid surface upon incidence of the nose shock on it. Thus, one would expect that the energy addition should be more or less concentrated, and that it should be positioned near the intersection of the nose shock with the upstream continuation of the cowl.

Note that heating and the resulting expansion of the gas would adversely affect both mass flow rate and stagnation pressure at the throat if the heated air is allowed to enter the inlet. Therefore, the energy addition region should be shifted somewhat down, so that heated and expanded air would miss the inlet, while cold air would be compressed and deflected into the inlet.

The qualitative expectations were confirmed in calculations, as illustrated in Figs. 14 and 15 for Mach 6, 1000 psf, zero angle-of-attack flight. In these calculations, circular-cylinder Gaussian heat addition, with $r_{\text{eff},x} = r_{\text{eff},z} = r_{\text{eff}} = 0.2$ m was assumed. (This value of r_{eff} was found to be close to the optimum.) In Fig. 14, the vertical location of the center of energy addition region was fixed at the cowl level, $z_Q = z_{\text{cl}}$, and in Fig. 15, the vertical location of the energy addition was shifted down by $2r_{\text{eff}} = 0.4$ m. In both Figs. 14 and 15, key inlet performance parameters are plotted vs horizontal coordinate of the energy addition center, at two values of the integral energy addition rate W. As seen in Figs. 14 and 15, energy addition does increase the mass capture, and the effect becomes stronger as more energy is added. Mass capture and the enthalpy flux both exhibit broad maxima at the value of x, approximately corresponding to the intersection of the nose shock with the upstream continuation of the cowl. Total pressure and adiabatic kinetic energy coefficients also have their peaks, but at a value of x somewhat shifted downstream with respect to that where mass capture is maximum. Because, however, the maximum of mass capture is very broad, a location maximizing both k_m and k_{p_t} can be reasonably selected. As predicted in the previous paragraph, shifting the center of energy addition region down from the cowl line somewhat improves inlet performance; indeed, maximum values of both k_m and k_{p_t} are greater in Fig. 15 than they are in Fig. 14. (Note that in calculations not shown here, we found that a shift by $2r_{\text{eff}} = 0.4$ m is near optimal, as moving the energy addition center farther downward decreases the performance.) At other Mach numbers and dynamic pressures, the behavior is similar to that depicted in Figs. 14 and 15. For example, Fig. 16 illustrates the Mach 8, 1000 psf case with energy addition center shifted down by $2r_{\text{eff}} = 0.4$ m. The maxima of inlet performance parameters here are even broader with respect to x than they are in Figs. 14 and 15. Static temperature contours and flow streamlines in the Mach 6, 1000 psf case with energy addition rate of $W = 10$ MW/m centered near the optimum location (see Fig. 15) are shown in Fig. 17, where the shock and flow patterns are seen to imitate those of the extended solid cowl case of Fig. 13.

The next issue addressed in our analysis was how the inlet performance would be affected if, instead of a single energy addition region, two energy addition regions are used with the total power equal to that of the single region. Figure 18 illustrates such a case, at Mach 6, 1000 psf, with two sources of 2.5 MW/m each. We found that, with proper positioning of the second source downstream of the first one, the inlet performance would not decrease compared with that given by a single of 5 MW/m. The same conclusion was reached at other Mach numbers, dynamic pressures, and total power levels.

We have also run a series of calculations with elliptical-cylinder Gaussian heating profiles. Stretching the energy addition profile along the flow, while maintaining constant total power, was found to result in a small improvement in inlet performance. Specifically, $r_{\text{eff},x} = 15r_{\text{eff},z}$ was found to give the best performance. We further found that slightly tilting the stretched heating profile with respect to

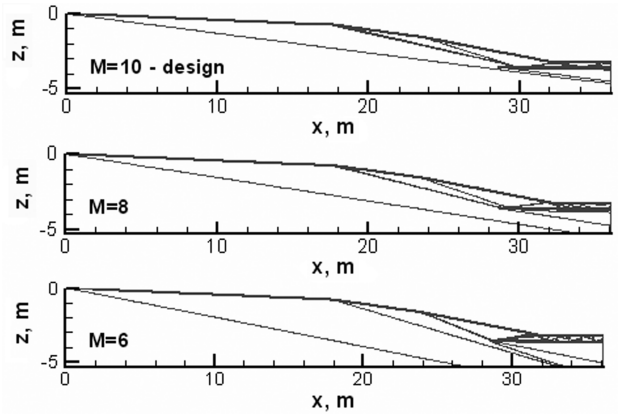

Fig. 11 Shock patterns (Mach number contours) at design Mach 10 and off-design Mach 8 and Mach 6 cases.

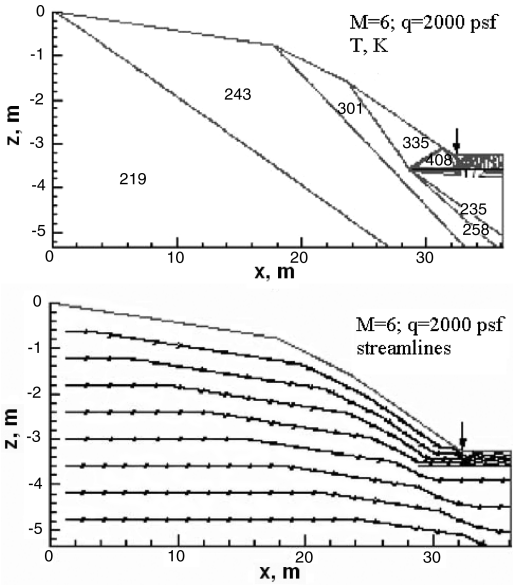

Fig. 12 Static temperature (upper plot) and flow streamlines (lower plot) in Mach 6, 2000 psf case without energy addition.

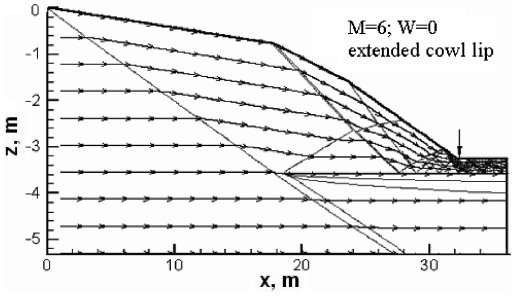

Fig. 13 Shock pattern and flow streamlines at Mach 6 with an extended solid cowl.

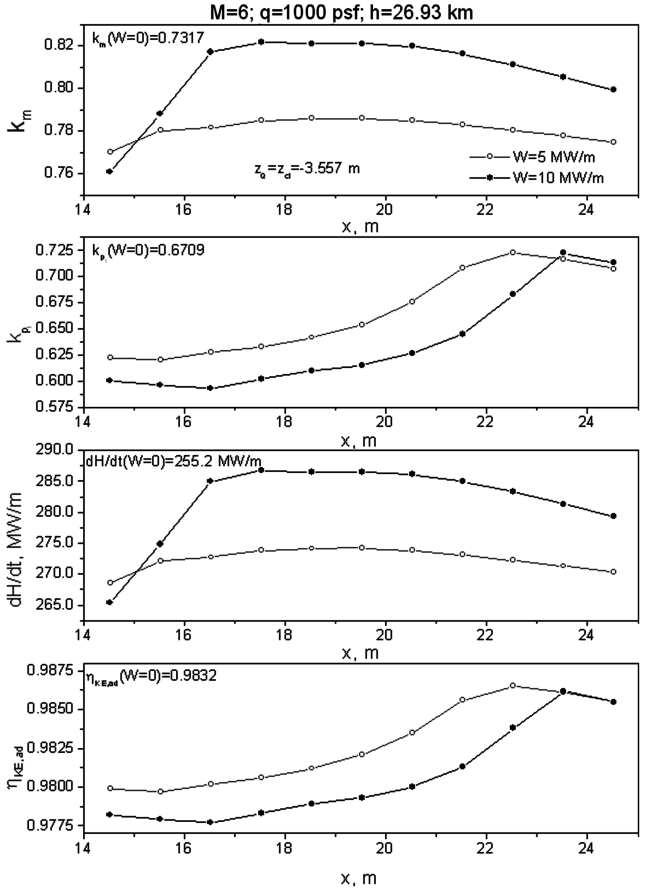

Fig. 14 Inlet performance parameters at Mach 6, 1000 psf, vs streamwise distance of energy addition region from vehicle nose, at two values of energy addition rate W. Energy addition profile is circular Gaussian with $r_{\text{eff}} = 0.2$ m, and vertical location z_Q of center of energy addition is fixed at cowl level z_{cl}. Values of performance parameters in absence of energy addition ($W = 0$) are indicated in upper left corners of the plots.

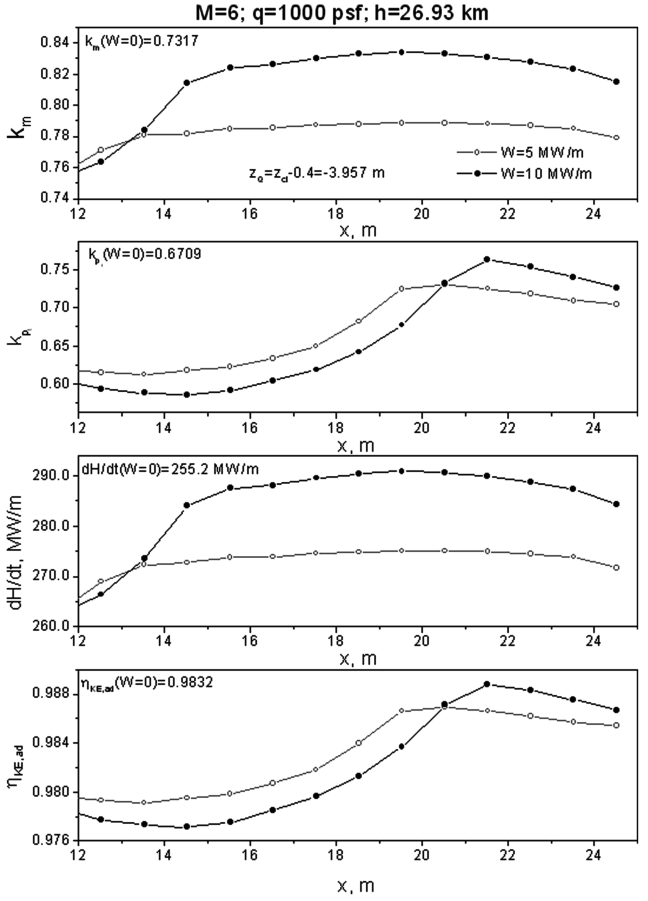

Fig. 15 Same as in Fig. 14, but vertical location z_Q of center of energy addition is fixed at 0.4 m below cowl level z_{cl}.

the x axis can improve the performance. The optimum angle turned out to be $\alpha_q = 2.5$ deg, which, perhaps not coincidentally, equals the angle of the first ramp. Figure 19 illustrates the optimum case with stretched and tilted heating profile at Mach 6. Overall, although stretched and tilted heating profiles do perform better than the "circular" ones, the improvement is only incremental.

For a virtual cowl created with plasmas, substantial quantities of electric power are required. If the virtual cowl needs to be created for a short time, a separate onboard power unit may be needed to use as an energy deposition source. Another possibility is to generate electric power by running an MHD generator downstream of the combustor. Whether the increase in engine performance given by virtual cowl (plus other improvements, such an increased lift) would outweigh thrust losses caused by the MHD power extraction should be studied in future.

Table 2 lists the most important computed cases and shows only the most important performance parameters. Table 2 also lists power deposition as a percentage of enthalpy flux into the inlet and inlet performance increase compared with that without heat addition. As can be seen in the table, optimally configured energy addition of only a few percent of the inlet enthalpy flux can increase both mass capture and compression ratio by 11–20%.

B. Shortening the Isolator by Heat Addition Upstream of Inlet Throat

As was mentioned earlier (Sec. III), the ramjet is only used to accelerate the vehicle up to about Mach 5 or 6, at which point the scramjet takes over. Cruise conditions are hypersonic: there is no design condition for the ramjet because it is only a transitional stage. A possibility to minimize the need for the traditional isolator stage using active control based on energy addition upstream of the inlet throat was theoretically explored in [30–33]. The energy addition can be accomplished by, e.g., microwave plasma heating, electron beams, or localized plasma-assisted combustion.

As described in [30–32], the inlet geometry was designed for the almost-shock-on-lip condition at a flight Mach number of 7 and dynamic pressure of 1000 psf (Fig. 20). In the off-design Mach 5 case with no heat addition, the stream-thrust averaged Mach number at the throat is 1.85, so that an isolator duct would normally be required to reduce the Mach number (as well as properly mix the flow). We then placed three distributed heating sources upstream of the throat, as shown in the upper plot of Fig. 21. The total heating rate is 20 MW/m (8.5% of the enthalpy flux through the throat), consisting of 13 MW/m between the cowl and the compression ramp, 5.25 MW/m at the cowl, and 1.75 MW/m at the ramp. The stream-thrust averaged Mach number at the throat is now 1.15, and the isolator duct can perhaps be eliminated. The computed inlet flow parameters are listed in Table 3.

These calculations demonstrate that, in principle, heating the flow upstream of the inlet throat can condition the flow in such a way that an isolator duct would be unnecessary. Practicality of this approach depends on whether the required amount of power can be generated and delivered at these relatively low flight Mach numbers, and whether the stagnation pressure losses in dissipative processes in the heated region and in the downstream MHD generator would still leave sufficient thrust to accelerate the vehicle.

C. Assessment of Performance of Reverse Energy Bypass Concept

One way of supplying the energy for the virtual cowl or inlet heating would be to extract energy from the flow with an MHD generator placed downstream of the combustor and deliver this energy to the desired location upstream of the inlet throat using dc,

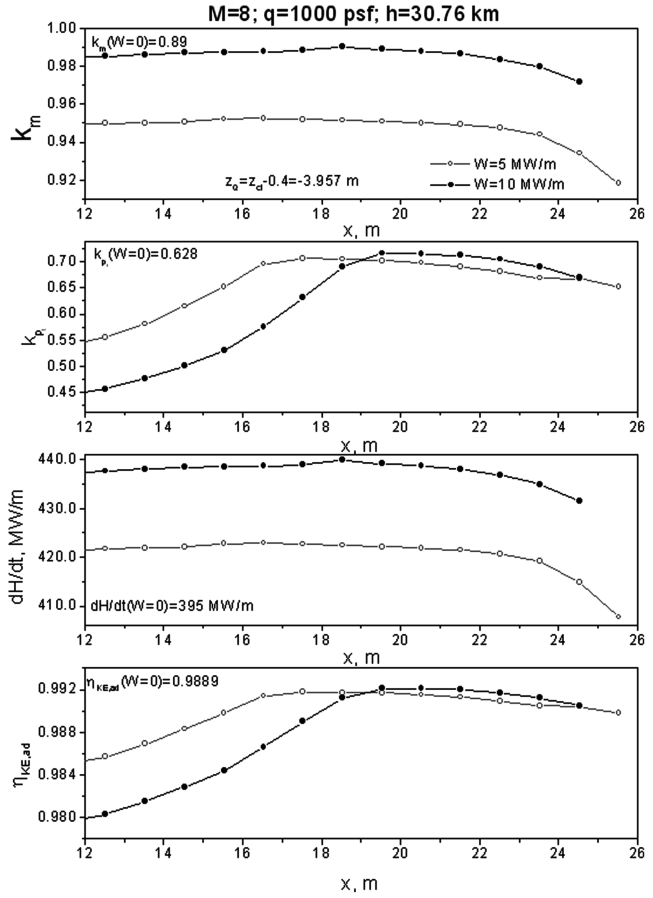

Fig. 16 Inlet performance parameters at Mach 8, 2000 psf, vs streamwise distance of energy addition region from vehicle nose, at two values of energy addition rate W. Energy addition profile is circular Gaussian with $r_{\text{eff}} = 0.2$ m, and vertical location z_Q of center of energy addition is fixed at 0.4 m below the cowl level z_{cl}. Values of performance parameters in absence of energy addition ($W = 0$) are indicated in upper left corners of the plots.

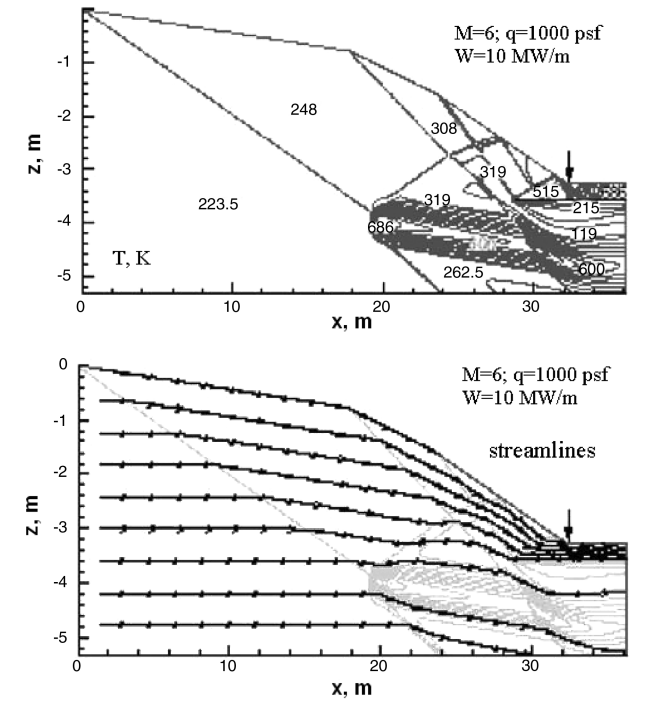

Fig. 17 Static temperature contour lines (upper plot) and flow streamlines (lower plot) at Mach 6, 1000 psf, with optimum location of circular Gaussian virtual cowl with $r_{\text{eff}} = 0.2$ m, $W = 10$ MW/m.

RF, or microwave plasma sources. In evaluation of the performance of this *reverse energy bypass concept*, losses of energy and stagnation pressure in all the system components must be taken into account.

In [31,32], we adopted a "linearized" approach, whereby percent changes of the thrust are calculated for each system component independently and the results are summed algebraically. This approach is obviously justified if the percent changes of the thrust are relatively small.

Parameters of the MHD generator placed downstream of the combustor were calculated for conditions corresponding to Mach 5 and Mach 6 flight at $q = 1000$ psf with the one-dimensional model of [30]. Combustor exit and MHD inlet conditions at Mach 5 and Mach 6 were those listed in [30] for a typical hydrogen-fueled ram/scramjet at the equivalence ratio of one. Potassium seed fraction in all cases was $\eta_K = 1\%$, and the load factor was either $k = 0.5$ or $k = 0.9$. The strength of the magnetic field was varied between 1.5 and 3.4 T. Note that in modeling the MHD generator, as well as subsequent flow expansion, enthalpy and entropy definitions were those used in chemical thermodynamics, including enthalpies of formation of mixture constituents. Therefore, the enthalpy extraction ratio values are different from values that would have been calculated if combustion were modeled as heat addition to a gas with constant composition. As shown in [31], an MHD generator with reasonable length (1 m), seed fraction (1%), and 1.5–3.4 T magnetic fields can indeed produce more than enough power to heat the flow upstream of the inlet and eliminate the need for an isolator duct (at least 20 MW/m), and to operate a virtual cowl for mass capture increase (at least 10 MW/m).

In thrust computations [31], friction and heat losses were neglected, and the flow from the combustor or MHD generator exit to the final exit plane (the vertical projection from the vehicle tail to the cowl line) was assumed one-dimensional, isentropic, and thermochemically equilibrium. Thus, the conditions at the final exit plane (index 2) are related to the conditions at the combustor or MHD generator exit (index 1) with the set of equations

$$\rho_1 u_1 a_1 = \rho_2 u_2 a_2 \qquad \frac{u_1^2}{2} + h_1 = \frac{u_2^2}{2} + h_2 \qquad s_1 = s_2 \qquad p_2 = \frac{\gamma - 1}{\gamma} \rho_2 h_2$$

where ρ is the density, p is the pressure, u is the velocity, h is the specific static enthalpy, s is the specific entropy, γ is the specific heat ratio, and a is the cross section area per unit length in the spanwise direction. The areas a were taken as $a_1 = z_{\text{in}}$ in the case with no MHD, $a_2 = z_L$ in MHD cases, and $a_2 = \Delta z_{\text{out}} = 8$ m. Thus, the overall area ratio $\Delta z_{\text{out}}/\Delta z_{\text{in}}$ between the final exit plane and the inlet capture plane was equal to two.

Because the parameters at the final exit plane varied within limited ranges, the approximation of ideal gas with constant specific heats was used for the equation of state at station 2. To find the necessary parameters for this equation of state, including the specific heats and the reference enthalpy and entropy, the ideal gas formulas were calibrated against ASTRA commercial software for calculations of

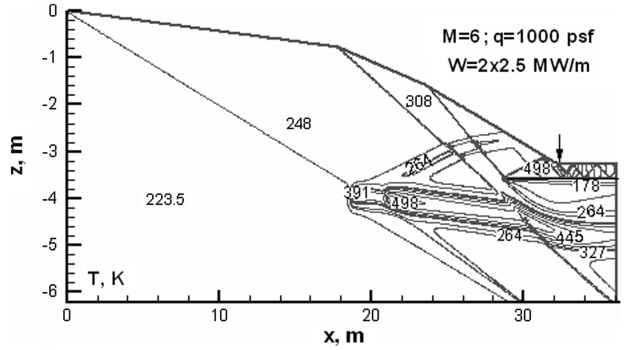

Fig. 18 Static temperature contour lines in Mach 6, 1000 psf case with two optimally located energy addition sources of 2.5 MW/m power each. Each source is circular Gaussian with $r_{\text{eff}} = 0.2$ m.

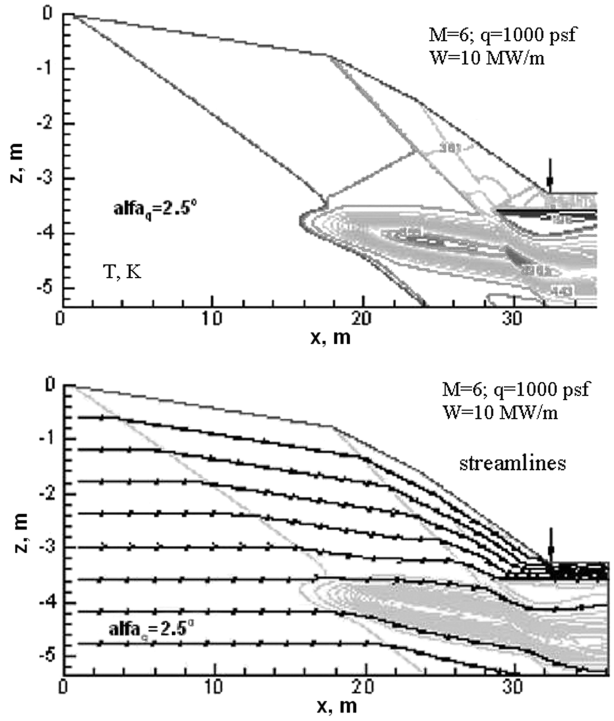

Fig. 19 Static temperature contours and flow streamlines at Mach 6, 1000 psf, with optimally located, stretched, and tilted 10 MW/m heating source (corresponding mass flow increase is 15.5%, and power deposition of 10 MW/m is ~3.4% of total enthalpy flux into inlet).

thermochemical equilibrium [49]. The calibration yielded the following parameters for the exit equilibrium stoichiometric hydrogen–air mixture:

$$\gamma = 1.3, \qquad c_p = 1442 \text{ J/kg}, \qquad h = c_p T - 3.75 \times 10^6 \text{ J/kg}$$

$$s = c_v \ln \frac{p}{\rho^{\gamma}} - 5051.18 \text{ J/kg}$$

With the fully specified flowfield, the sums of the pressure force and the momentum flux at the inlet capture plane, $F_1 = k_m(\rho_0 u_0^2 + p_0)\Delta z(0)$ with $\Delta z(0) = 4$ m (k_m is the inlet mass capture coefficient) and at the final exit plane, $F_2 = (\rho_{\text{out}} u_{\text{out}}^2 + p_{\text{out}})\Delta z_{\text{out}}$, were computed. The thrust was then found as $F_2 - F_1$. For example, in the design regime at Mach 7, $q = 1000$ psf, $F_1 = 378656.7$ N/m, $F_2 = 528375.8$ N/m, and $F_2 - F_1 = 149719.1$ N/m.

To evaluate thrust changes due to the inlet heating, the values of mass capture coefficient k_m, enthalpy capture coefficient k_H, and kinetic energy efficiency $\eta_{\text{KE,ad}}$ were used together with the sensitivities of the thrust with respect to these parameters provided by D. Van Wie of Johns Hopkins University Applied Physics Laboratory. The resulting change in thrust due to the 20 MW/m inlet heating was estimated to be about −5% (for details, see [31,34]). The

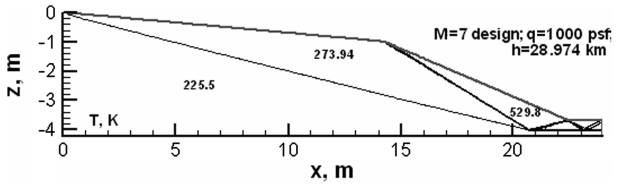

Fig. 20 Contour lines of static temperature in Mach 7, $q = 1000$ psf design case.

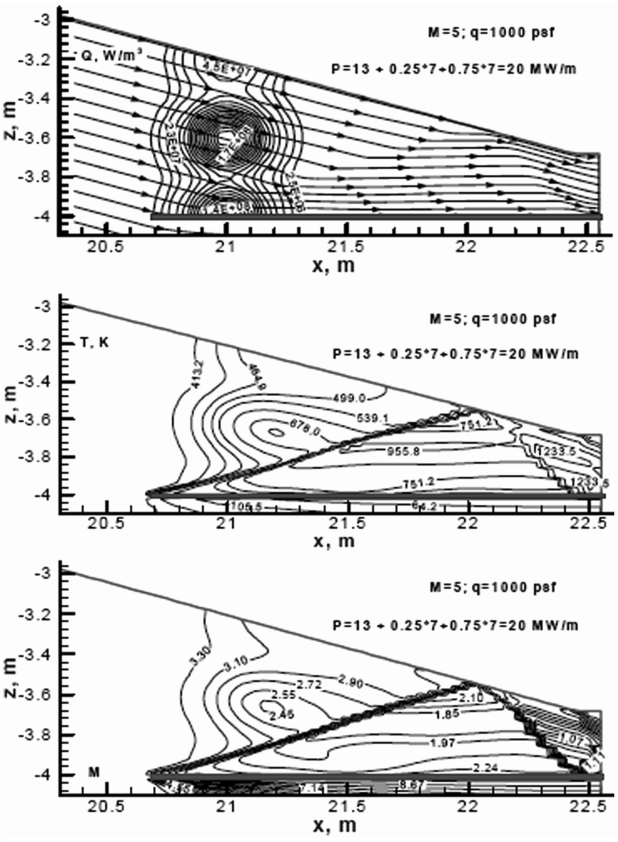

Fig. 21 Power deposition density, contour lines of static temperature and Mach number, and flow streamlines in Mach 5, 1000 psf off-design case. Total heating rate is 20 MW/m (8.5% of enthalpy flux through throat), consisting of 13 MW/m between cowl and compression ramp, 5.25 MW/m at the cowl, and 1.75 MW/m at the ramp.

overall performance of the energy bypass system with inlet heating depends on the efficiency of transmission of MHD-generated power to the inlet heating plasma. Because the inlet heating occurs in a duct, a dc or RF plasma can be run with direct connection to the MHD generator, so that nearly all generated power can be deposited in the

Table 2 Summary of principal cases and principal performance parameters for computed virtual cowl cases [power deposition as percentage of enthalpy flux into the inlet, and performance increase (in percent, compared with the cases with $W = 0$ and no extended cowl) are also indicated]

	Mach number and energy addition rate	k_m	k_p	η_{KE}	$\dot{H}$, MW/m
	$M = 10$	0.955	41.26	0.992	523.26
$M = 8$	$W = 0$	0.889	38.86	0.989	395.0
	$W = 0$, ext CL	0.98 (+10.2%)	42.538 (+9.5%)	0.991	435.3 (+10.2%)
	$W = 5$ MW/m, 1.2% $\dot{H}$	0.952 (+7.1%)	40.938 (+5.3%)	0.991	423.0 (+7.1%)
	$W = 10$ MW/m, 2.3% $\dot{H}$	0.99 (+11.4%)	43.561 (+12.1%)	0.991	439.8 (11.3%)
$M = 6$	$W = 0$	0.731	31.6	0.983	255.2
	$W = 0$, ext CL	0.981 (+34.2%)	44.78 (+41.7%)	0.992	342.4 (+34.2%)
	$W = 5$ MW/m, 1.8% $\dot{H}$	0.788 (+7.8%)	33.85 (+7.1%)	0.987	275.0 (+7.8%)
	$W = 10$ MW/m, 3.4% $\dot{H}$; $r_{\text{eff},x} = 0.2$ m, $r_{\text{eff},z} = 0.2$ m	0.833 (+13.9%)	33.68 (+6.6%)	0.983	290.8 (+13.9%)
	$W = 10$ MW/m, 3.4% $\dot{H}$; $r_{\text{eff},x} = 3$ m, $r_{\text{eff},z} = 0.2$ m $\alpha_q = 2.5$ deg	0.844 (+15.5%)	37.8 (+19.6%)	0.986	294.5 (+15.4%)
	$W = 35$ MW/m, 10.2% $\dot{H}$; $x_Q = 18.5$ m, z_{CL}-$z_Q = 1.3$ m	0.983 (+34.5%)	52.73 (+66.9%)	0.980	342.9 (+34.4%)

Table 3 Computed cases and principal performance parameters for inlet/isolator control with energy addition or on ramp MHD: mass capture k_m, compression ratio k_p, adiabatic kinetic energy efficiency $\eta_{KE,ad}$, average Mach number at the throat $\langle M \rangle$, enthalpy capture ratio k_H, and the enthalpy flux through the throat $\dot{H}$

Flight Mach number, dynamic pressure, and energy addition rate (power)	k_m	k_p	$\eta_{KE,ad}$	$\langle M \rangle$	k_H	$\dot{H}$, MW/m
$M = 7$, $q = 1000$ psf, Power = 0 (design)	0.957	61.4	0.970	2.81	1	425.9
$M = 4$ Power = 0	0.55	45.89	0.958	1.1	1	180.75
$M = 5$ Power = 0	0.679	43.71	0.958	1.85	1	232.4
Inlet Mach number reduction by heat addition upstream of the throat						
Power $= 10.5 + (0.75 \times 4.5)_{cowl} + (0.25 \times 4.5)_{ramp} = 15$ MW/m $= 6.3\%\dot{H}$	0.65	67.56	0.914	1.3	1.07	236.3
Power $= 13 + (0.75 \times 7)_{cowl} + (0.25 \times 7)_{ramp} = 20$ MW/m $= 8.5\%\dot{H}$	0.63	78.79	0.9023	1.15	1.092	234.4

inlet. To minimize stagnation pressure losses in the MHD generator due to dissipative joule heating, the load factor should be close to one, and to maintain the extracted power, the magnetic field should be increased. For example, with $k = 0.9$ and $B = 2.5$ T, thrust reduction (−14%) is somewhat lower than with $k = 0.5$ and $B = 1.5$ T (−16%) [18]. The 14–16% reduction in thrust can leave enough thrust to accelerate the vehicle, while eliminating the isolator duct and thus increasing performance at cruise [31,34].

In assessing the performance of the reverse bypass system with an MHD generator powering a virtual cowl, the results of the evaluation of virtual cowl effect on thrust performed by D. Van Wie of Johns Hopkins University Applied Physics Laboratory [30] were used. Specifically, as shown in [30], the increase in thrust is nearly equal to the increase in mass capture coefficient due to virtual cowl. In the case of a virtual cowl in its optimum location, far from the vehicle surface (Figs. 17–19), the required energy would have to be deposited by, e.g., freely localized plasma created by a phased microwave array. In this case, the efficiency of energy transmission from the MHD generator to the freely localized microwave plasma would be quite low, perhaps as low as 25%: for a 10 MW/m heating, about 40 MW/m would have to be generated. With a virtual cowl located close to the cowl lip, dc or RF discharges could also be conceivably run. In the latter case, 54% power transmission efficiency was assumed in the calculations [31]. As shown in [31], the increase in thrust due to virtual cowl is somewhat reduced because MHD generation of power required for virtual cowl entails substantial reduction in thrust, both because of the need to generate enough power to compensate for conditioning and transmission losses and due to the dissipative joule heating. Overall, the best performance for the reverse energy bypass with optimally located virtual cowl is 9.4% thrust increase, whereas thrust increase with virtual cowl close to the cowl is around 6.5% [31].

D. Energy Addition Ram/Scramjet Propulsion Control: Concluding Remarks

We explored the concept of ram/scramjet propulsion control by energy addition and extraction in the propulsion flowpath. Instead of variable geometry, the concept relies on virtual shapes created by plasma/MHD devices or by other methods (including plasma-controlled combustion). An inherent advantage of the proposed plasma/MHD control system is its flexibility, fast response, and the absence of moving parts. At Mach numbers higher than the design value, an MHD generator placed at the first compression ramp and using ionization by electron beams can restore the shock-on-lip condition, while operating in self-powered regime (see review papers [44]).

At Mach numbers below the design value, inlet performance can be controlled by energy addition, with the power supplied by an MHD generator placed downstream of the combustor. This concept is called the reverse energy bypass. In one scenario, the inlet flow spillage can be reduced by virtual cowl: a heated region placed upstream of the cowl and slightly below it. The optimum location of the virtual cowl is such that the shock generated by the energy addition passes through the point where the nose shock intersects with the upstream continuation of the cowl line. Stretching and tilting the energy addition region can improve performance, although incrementally. Energy addition far from the vehicle surface can also improve performance, but only slightly, and the improvement would probably be negated by technical difficulties in depositing and controlling a large amount of energy far from the vehicle surface. Thus, the best location for the virtual cowl appears to be at or slightly below the cowl line. The modeling results considered earlier demonstrates that a virtual cowl created by energy deposition upstream of the cowl lip can substantially increase mass capture and kinetic energy efficiency of the inlet. The performance of virtual cowl can approach or match that of a would-be upstream solid extension of the cowl. With the power deposition of only 2–3.5% of the enthalpy flux into the inlet, the mass flow rate entering the inlet and the compression ratio can be increased each by 15–20% (at Mach 6), with no loss of kinetic energy efficiency.

The physical mechanism of energy addition was not analyzed in this paper. Among possible candidates, hot-air jets or plasma-controlled external combustion can be considered. Plasma methods potentially include initiating and controlling ionization by laser sparks of magnetically guided electron beams, and depositing energy by non-self-sustained (subcritical) RF or microwave sources. Note that some inlet designs contain sidewalls extended upstream of the cowl lip [28]. If the sidewalls are extended far enough, they could be used to carry the hardware (electrodes, wiring, electron guns, magnetic coils, etc.) for plasma methods of generation of virtual cowl. Shooting combustible liquid or solid pellets [48] in the upstream direction may be an interesting option.

For a virtual cowl created with plasmas, substantial quantities of electric power are required. If the virtual cowl needs to be created for a short time, energy stored or generated with a separate onboard power unit might be used. Another possibility is to generate electric power by running an MHD generator downstream of the combustor.

In another scenario, distributed heating of the flow upstream of the inlet throat in the ramjet regime (Mach 4–6), with the heating rate of about 6.3–8.5% of the total enthalpy flux, can bring the throat Mach number close to one, thus making the isolator duct virtually unnecessary. Although the reverse bypass system with inlet heating would reduce thrust by about 16% at Mach 5, the performance penalty at the vehicle acceleration stage can be offset by the increased efficiency during the cruise due to the absence of weight and cooling burden normally caused by the long isolator duct. As an added benefit of inlet control by plasma energy addition, generation of active radical species in the plasma region would mitigate the ram/scramjet combustion ignition problem. In the reverse bypass concept, MHD generation of power required for inlet control entails substantial reduction in system performance, both because of the need to generate enough power to compensate for conditioning and transmission losses and due to the dissipative joule heating. The latter can be minimized by operating with a load factor close to one with the appropriate increase in magnetic field strength to maintain the required power level.

To assess the impact of plasma and MHD control devices on the overall vehicle performance, it would be desirable to develop a simple computational code for "tip-to-tail" flowpath analysis. To be useful for design purposes, the code is designed to be simple, that is, it is based on ordinary differential and/or algebraic equations, and

modular (so that various parts and devices could be included or excluded and their parameters varied independently), while capturing the essential physics of flow, combustion, and plasma processes. Discussion of such a code was presented recently in [32]. Because standard codes for supersonic diffusers with oblique shocks cannot be applied to the cases with plasma heating and/or chemical reactions, we have proposed a method whereby the results of 2-D modeling are compared with 1-D shock-free flow, and a set of matching coefficients is derived and then used in quasi-one-dimensional modeling [32].

IV. Aerodynamic Forces Created by Off-Axis Heat Addition Upstream of a Body

In the case of off-axis power deposition upstream of the body of revolution, pressure distribution on the body surface becomes asymmetrical, and steering or lifting moments can be created.

Girgis et al. [50] carried out a fully three-dimensional inviscid numerical simulation to understand and determine the effect of heat addition upstream of a 15 deg half-angle cone at Mach 3 on drag reduction and creation of steering force. A nondimensional parametric study was conducted to examine the effect of different parameters on drag and lift of the body. This includes heat deposition region location, (distance from the tip of the body R and angle θ), effective heating radius r_{eff}, freestream Mach number M_∞, and the power of heat deposition source P, as shown in Fig. 22.

The governing equations were discretized using a second-order, cell vertex, finite volume scheme in space. Integration of the governing equations in time, using a four-stage Runge–Kutta scheme, was employed until a steady-state solution was reached. Both spherical Gaussian and realistic electron-beam-controlled microwave heating profiles were used.

In result of a series of computations, was found the optimum distance, effective heating radius and angle, off the cone axis, θ, to generate steering moment. For $M_\infty = 3.0$ and heat source power P: $P/P_D = 1.0$ ($P_D = 0.5\rho_\infty u_\infty^3 A$), it was found that optimal parameters are $R/D_{\text{opt}} \sim 0.4$, $r_{\text{eff}}/D = 0.2$, and θ_{opt} between 40 to 50°, deg, where D is the diameter of the cone, u_∞ is the freestream velocity, ρ_∞ is the freestream density, and A is the cone cross-sectional area. The maximum drag reduction $C_D/C_{D0} = 0.65$ occurs at $\theta = 0$. The optimum case for drag reduction is shown in Fig. 23, where the nondimensional pressure distribution p/p_∞ is plotted on the left. The heat addition region acts as an obstacle shielding the cone from the upcoming high-speed flow and deflects the flow away.

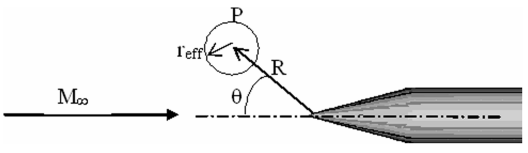

Fig. 22 Variables of parametric study.

In practice, local energy addition to the flow can be achieved by the use of microwave radiation as a heating source and an e beam to control the air conductivity and the corresponding location of the energy deposition. Because steering requires concentrated heating in a localized preionized region, the strength of the microwave field needs to be much lower than the critical value of the electric field at breakdown. When the spatial profile of the electron beam and the microwave-induced heating was considered, the optimum electron beam angle was found to be around 60 deg. Because the electron beam heating profile is not concentrated as much as the spherical Gaussian heating profile, the corresponding drag reduction and steering force gain ($C_D/C_{D0} = 0.37$ and $C_L/C_D = 0.42$) are not as large as those obtained with the spherical Gaussian heating profile, as shown in Fig. 24.

Finally, in [50], the effect of Mach number on the steering force was studied. Figure 25 shows the substantial effect of Mach number increase on the steering force. Because it takes numerous simulations to obtain the optimum heating location, the results at $M_\infty = 5.0$ was not as well optimized as that of $M_\infty = 3$ and 2.4. It is clear that a considerable gain in steering moment can be achieved at high Mach numbers. Because the pressure jump across a shock wave is proportional to M_∞^2, at high Mach numbers, the drag reduction due to heating and a corresponding Mach number change ΔM are approximately proportional to $2M_\infty \Delta M$, where, as discussed by McAndrew [51], for a simple Rayleigh flow at fixed static pressure and volumetric heat addition, ΔM is a weak function of Mach number. Figure 25 supports this approximation and shows that C_L/C_D increases approximately linearly with Mach number. Thus, heat addition for the improvement of vehicle performance becomes more efficient at elevated Mach numbers, corresponding to hypersonic speeds.

A small scale wind tunnel for studies of aerodynamic control using heat addition and for measurements suitable for comparison with computational fluid dynamics (CFD) calculations was designed and built in Princeton [51,52]. The conditions of the CFD calculations previously presented are the same as in the experiments (Mach 3 wind tunnel with a 15 deg half-angle instrumented cone used to measure aerodynamic forces). Freestream heat addition was achieved by the microwave-driven discharge. Microwave plasmas were initiated by an electron beam injected into the flow through the test section wall. A photograph of the plasma and the test section from the experimental work done by McAndrew et al. [52] is shown in Fig. 26. The flow is from left to right and the cone can be seen on the right-hand side.

Lift and drag changes over the cone were measured with the force balance. Experiments demonstrated changes in lift and drag as functions of microwave power with an off-axis plasma location. Figure 27 shows the results obtained by McAndrew et al. [51,52] for

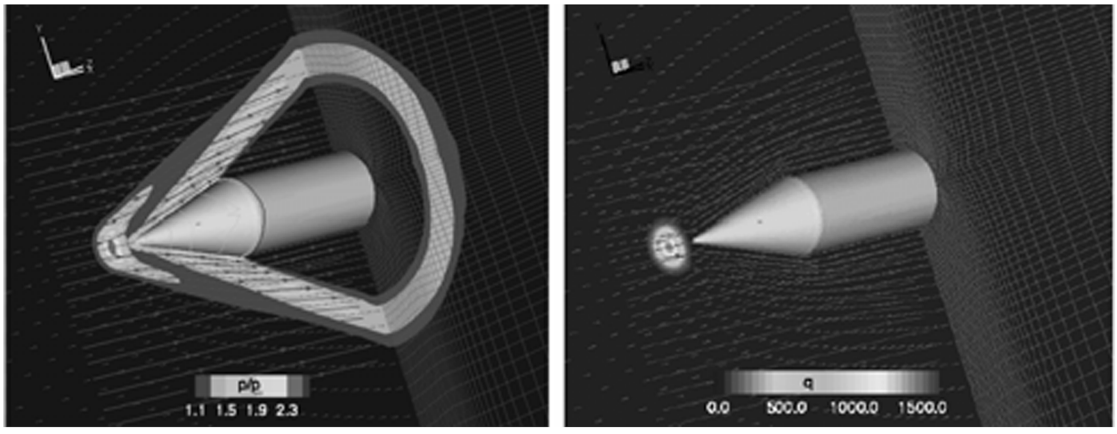

Fig. 23 Pressure distribution (left) and power density distribution (right) in flow over a cone. Drag reduction, optimum case ($M_\infty = 3.0$, $P/P_D = 1.0$, $R/D = 0.408$, $\theta = 0$ deg, $C_D/C_{D0} = 0.65$, and $C_L/C_D = 0.00$).

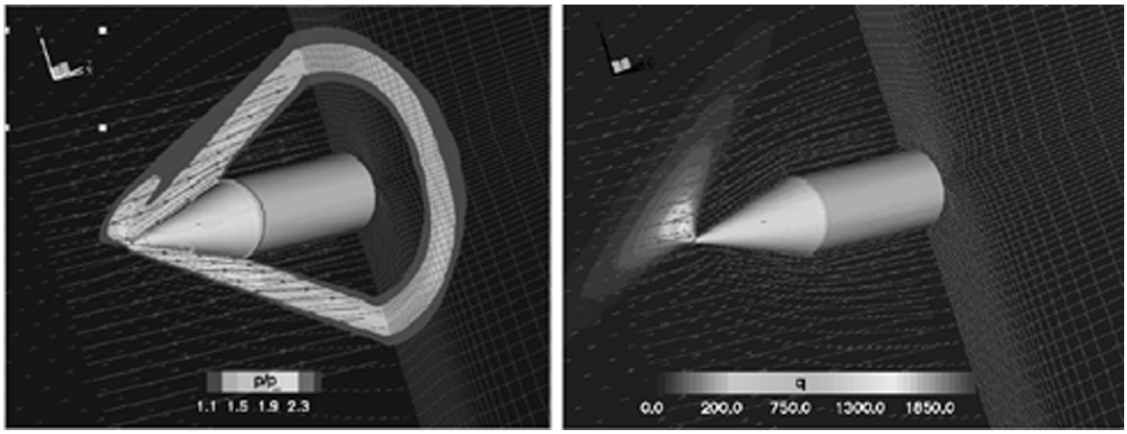

Fig. 24 Pressure distribution (left) and power density distribution (right) in flow over a cone, using electron beam and microwave-induced heat addition. Creation of steering force, optimum case ($M_\infty = 3.0, P/P_D = 1.0, L_{\text{ext}}/D = 0.2, \theta = 60$ deg, electron beam energy $= 20$ keV, $C_D/C_{D0} = 0.37$ and $C_L/C_D = 0.42$).

the lift coefficient C_L vs the normalized power (P/P_D). These results are in reasonable agreement with the computations [53].

A larger lift coefficient for the CFD prediction is obtained because, in the calculations, it is much easier to optimize both the heat addition profile and its location.

V. Energy Addition in Supersonic Flows for Sonic Boom Mitigation

Shock waves generated by a supersonic object are known to produce a sonic boom on the ground. Sonic boom formation has been the main obstacle in the development of commercial supersonic vehicles. For a supersonic aircraft, the near-field shock structure is a complex array of shock waves that originate from various parts of the aircraft. In the far field, these shock waves coalesce and produce an *N*-shaped pressure signature on the ground. Although the sonic boom is a far-field phenomenon, several near-field techniques have been suggested to attenuate the shocks with the assumption that it will eliminate or partially reduce the sonic boom on the ground. These techniques include the design of exceptionally long aircraft [53,54], use of underwing thermal gradients [55], and the possibility of high-speed oscillations of flight velocity [56]. Current work focuses mainly on the development of long, thin aircraft because the other methods seem unrealistic due to practical considerations. Energy addition is an alternative approach to sonic boom mitigation. It has been argued that upstream energy addition to a supersonic vehicle may weaken the shock wave and may prove to be a useful approach to suppress the sonic boom on the ground. Recent work related to the Defense Advanced Research Projects Agency's (DARPA) Quiet Supersonic Platform program, which was conducted at Princeton, addressed these issues in some detail. The details of this project have been presented by Miles et al. [57]. The results indicated that steady-state off-body energy addition can reduce the far-field signature primarily by suppressing the far-field coalescence of the shock waves originating from the various parts of the vehicle [57].

The dynamic effects of energy addition were investigated with a time-marching Euler code based on the second-order MacCormack method on a rectangular grid. Preliminary modeling was performed in two dimensions with the energy added along a line across the two-dimensional domain and the effects seen on the shock structure from a wedge. The simplicity of this configuration allows the code to follow the dynamics of the interaction of the energy addition with the

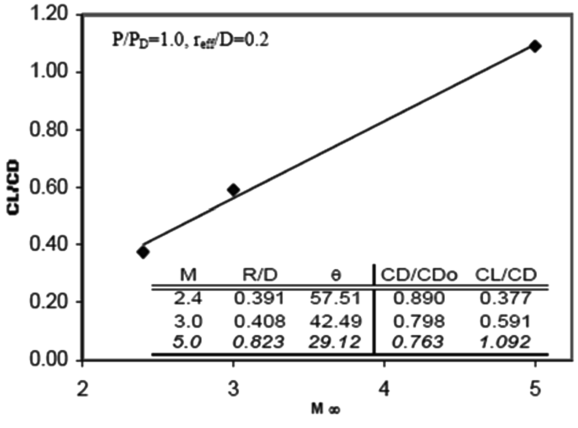

Fig. 25 Mach number effect on steering force.

Fig. 26 Plasma over 15 deg cone in Mach 3 flow [54,55].

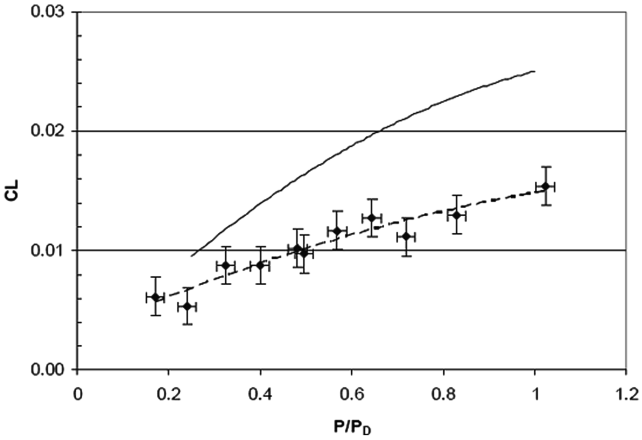

Fig. 27 Lift coefficient vs normalized power (McAndrew et al. [51,52]); solid line: calculations (Girgis et al. [50]).

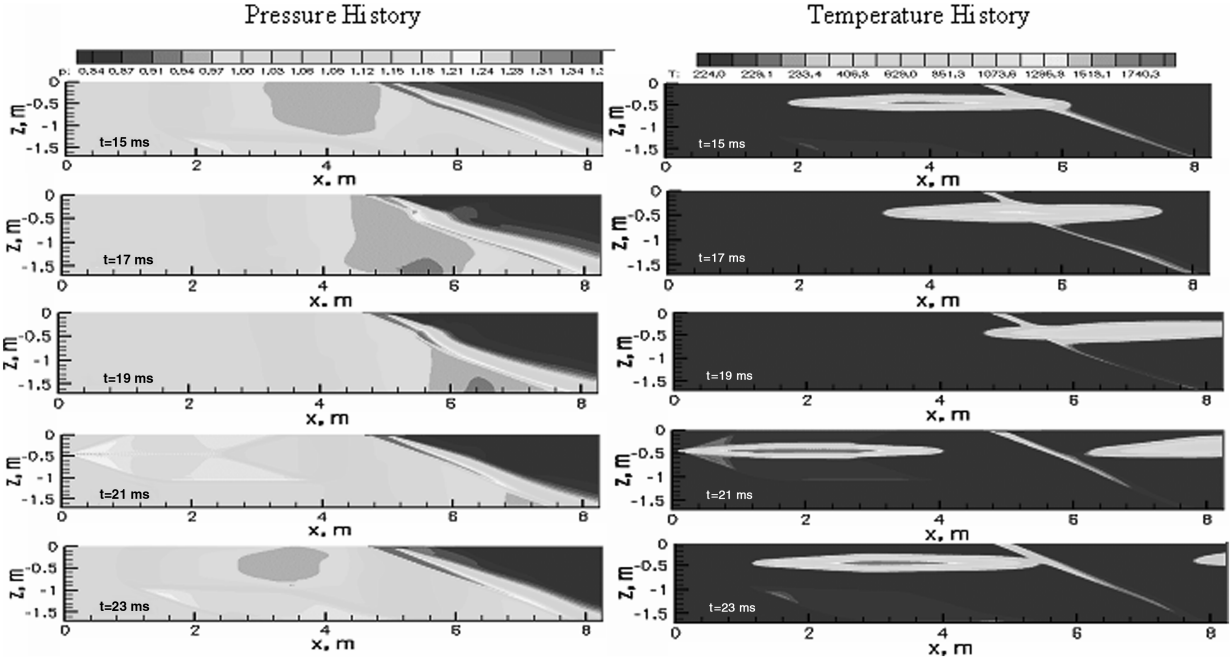

Fig. 28 Two-dimensional, time-accurate model of pulsed energy addition. Flow is from left to right. Energy addition regime modulates and weakens bow shock.

bow shock. An example of the interaction of a series of energy addition pulses is shown in Fig. 28. These are five frames from a movie that show the dynamics of the interaction. Figure 29 shows the impact of those pulses on the pressure measured at the bottom of the frames shown in Fig. 29 ($z = -1.6$ m). In the absence of energy addition, the bow shock produces a $P_{\max}/P_0$ of 0.027 which is shown by the arrow on the left side of Fig. 29. In the presence of the pulsed energy addition, the $P_{\max}/P_0$ from the bow shock oscillates, but is consistently lower in value than it is in the absence of the energy addition. The bow shock pressure is modulated in time (solid line), but the averaged pressure amplitude from the bow shock is 20% lower than the steady-state one without the heat addition (shown by the arrow). The energy addition process itself generates an oscillating shock, but that is significantly weaker, as shown by the dotted line. It is expected that the addition of energy by pulses such as this will reduce the total power requirements for modifying the far-field signature, and it may introduce new effects that further suppress the far-field coalescence and reduce sonic boom. These dynamic far-field effects cannot yet be predicted and have not yet been measured [56].

The preceding example explicitly demonstrates the significance of energy addition to control flowfields around objects flying at supersonic or subsonic speeds. Among various methods of energy addition, laser initiated optical discharges have been found to be an efficient way to control the position and structures of shock waves [15,58,59]. In this regard, laser-based energy addition techniques find an important application in the area of sonic boom mitigation. To demonstrate this approach and to investigate the dynamic effects of energy addition upstream of the shock wave produced by a model in the flow, experiments were performed under DARPA's Quiet Supersonic Platform program at Princeton.

The experimental program was established to validate model predictions for the dynamic energy addition and to examine the real-time near-field interaction of the energy addition with the shock wave produced in the flow. A Mach 2.4 nozzle was designed to perform experimental studies. A model was placed in the test section (length = 6 in., width = 2.15 in., height = 1.9 in.) to produce a shock wave. The static pressure in the test section was near atmospheric to permit localized energy addition by laser-induced breakdown. A 10 Hz Nd:YAG laser was employed to add energy into the flow. The pulse energy was about 350 mJ/pulse, and a 100 mm

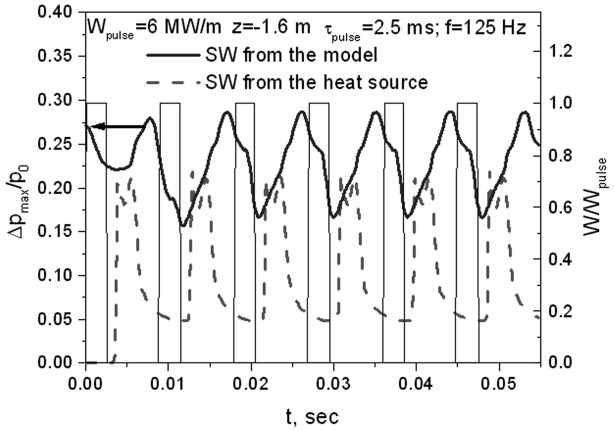

Fig. 29 Maximum relative pressures at bottom cross section: $z = -1.6$ m on Fig. 29. Rectangles show energy addition pulses in relative units. Bow shock pressure is modulated in time (solid line), but averaged pressure amplitude from bow shock is 20% lower than steady-state one without heat addition (shown by arrow). Pressure associated with shock generated by heat addition is shown by dotted line and maximal pressure from heat source is significantly lower than one from the model; pulse duration $\tau_{\text{pulse}} = 2.5$ ms, frequency $f = 125$ Hz.

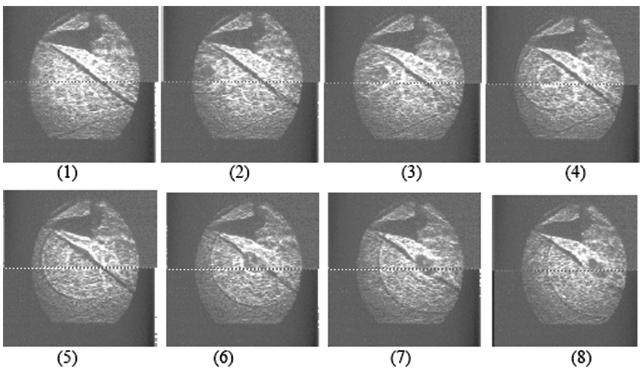

Fig. 30 Shadowgraph images of interaction between laser thermal spot and oblique shock wave from a wedge in Mach 2.4 flow. Images are 8 μs apart.

focal length was used to obtain breakdown in the region of interest upstream of the model. A Princeton Scientific Instrument ultrafast framing camera (PSI-4) was used to capture the shock wave interactions in the test section as the energy is added to the flow. Figure 30 shows the experimental results [60,61], as the shadowgraph images that were captured with the desired flow in the tunnel. Flow is from left to right, and the laser was focused at the position mentioned in Fig. 30. The frame integration time was 2 μs. Frames in Fig. 30 clearly show the thermal spot along with its associated shock wave propagating with the flow. As the thermal spot passes through the oblique shock, a significant distortion and weakening of the shock can be seen in frames 4–7. Full details on these experiments can be found in [60,61]. It is important to note that for an effective sonic boom reduction, the position of the laser breakdown spot should be optimized so that the shock wave generated by the thermal spot weakens before it reaches the bow shock. In this case, the interaction of the thermal spot would have a more pronounced impact on the bow shock.

Modeling was conducted at the flow conditions used for the experimental studies ($M = 2.4$, $P_0 = 1$ atm, $T_0 = 136$ K, $\gamma = 1.4$). A time-marching, two-dimensional Euler code was used for this purpose. Computations were performed by the second-order MacCormack method on a rectangular grid. The energy deposition region was assumed to have a cylindrical shape and a Gaussian distribution in the (x, y) plane with an effective radius of 0.125 cm. This assumption was based on the fact that a laser spark produces a cylindrical shock wave and a rarefied thermal spot, both of which move downstream with the flow.

Figure 31 presents the computational results describing the dynamics of interaction of the energy addition with the shock wave generated by the model. The energy addition itself generates a shock wave that grows as it propagates in the flow. Frames in Fig. 31 clearly show the complex interaction of the entropy spot with the oblique shock, and also show attenuation of the shock wave as it passes through the entropy spot. Figure 31 also shows the way the laser-generated shock wave gets reflected from the model surface, which makes the dynamics of interaction even more complex.

Calculations were performed for the interaction of the flow-convected thermal spot with and without the accompanying shock wave with the oblique shock from the model. A remarkable difference between the two cases can be seen in terms of pressure variation along the surface of the test section, as shown in Fig. 32. In the case when the laser spot is focused 10 mm upstream and 10 mm below the model, the pressure variation is maximum. The rise in pressure is due to the interaction of the shock wave surrounding the thermal spot with the oblique shock wave, whereas the pressure decreases when the thermal spot interacts with the model shock. Because pressure calculations were made in the near field, only 2.5 cm below the model, the interaction of the shock waves with the expansion fan located at the far right edge of the model affects the pressure in a complex fashion. Because of this, several fluctuations in the pressure curve can be seen in Fig. 33. As the laser spark is moved farther away from the model edge (40 mm upstream), the shock wave around the thermal spot becomes weaker and the corresponding pressure variations become smaller in amplitude, as can be seen in Fig. 33. For the isobaric case, the pressure inside the energy

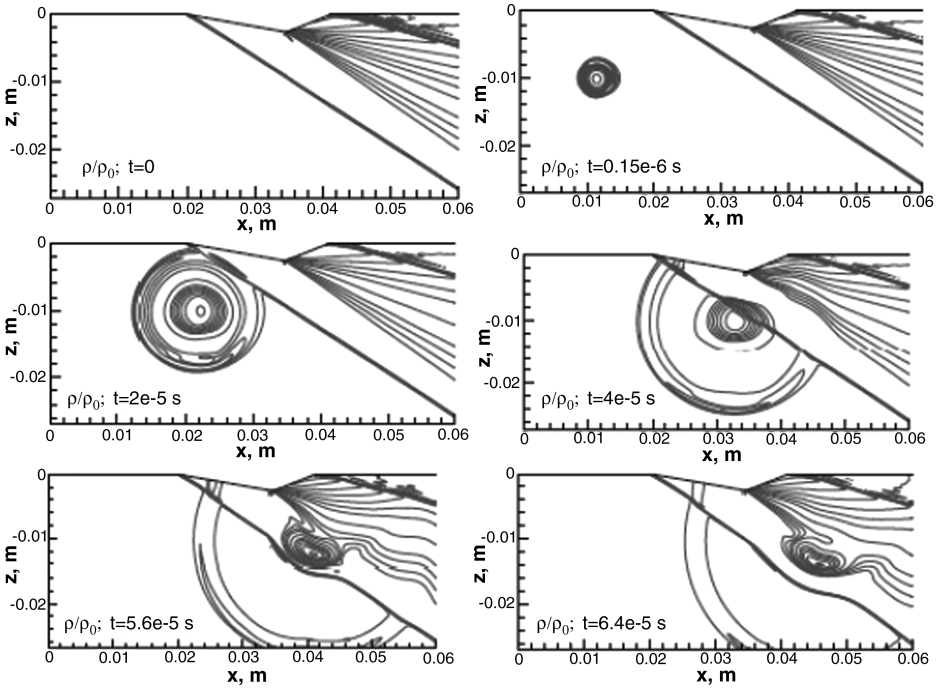

Fig. 31 Two-dimensional, time-accurate model of laser spark and oblique shock wave interaction (density contours). Flow is from left to right.

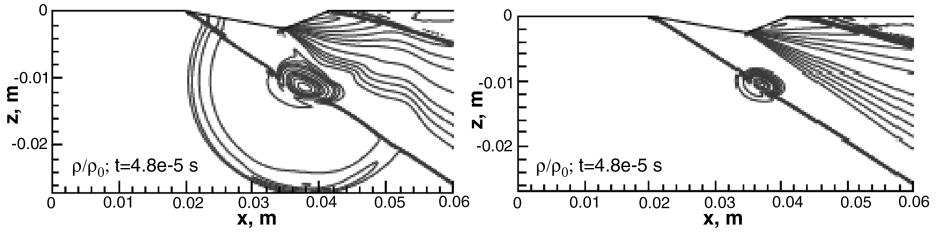

Fig. 32 Cylindrical shock wave and thermal spot interaction with the oblique shock at $t = 48$ μs after the laser spark (left), and the thermal spot-oblique shock interaction at the same time moment (right).

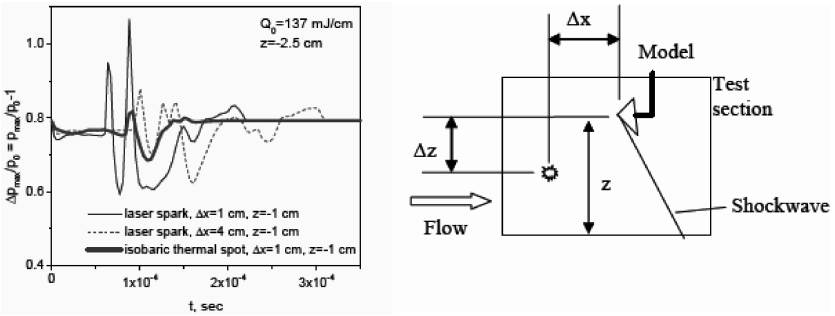

Fig. 33 Computational predictions of maximum relative pressures at bottom of test section for various energy addition positions (left), and geometry indicating position for localized energy addition to predict pressure variations at bottom of test section (right).

deposition has been assumed constant (thermal spot without the surrounding shock wave). In this case, only the interaction of the thermal spot has been analyzed, and the pressure associated with the oblique shock wave was reduced without large fluctuations.

Thus, the position of the laser breakdown spot should play a vital role in the mitigation of shock waves and of the sonic boom from a supersonic vehicle. Far-field experiments will be required to demonstrate the effectiveness of this technique.

The results of both experiment and numerical modeling [60,61] clearly demonstrate the strong influence of the pulsed power deposition in supersonic flow on shock wave intensity in the near field of the body. Determining whether the problem of sonic boom mitigation in the far field can be solved by such means requires additional theoretical and experimental investigations. It is possible that the "quiet" power deposition (a long, thin heated region with low-power input per unit volume) suggested by Kolesnichenko et al. [25,26] and by Georgievsky and Levin [27] can be useful, not only for drag reduction, but also for sonic boom mitigation, because in that case most of the power is spent on creation of the thermal wake, rather than on generating shocks.

VI. Conclusions

This paper presents a short selective review of several important examples of supersonic and hypersonic flow control by energy deposition. The examples demonstrate that energy addition to the flow, with the proper optimization, can successfully address problems of supersonic/hypersonic drag reduction, steering, increasing mass capture in scramjet inlets, and sonic boom mitigation. All of these problems and methods are multidisciplinary by their nature, and their further development requires concerted research efforts in various fields: experimental and computational fluid dynamics, plasma physics and chemistry, electrical engineering, etc. Whether or not these methods could become practical should be determined by system studies.

Acknowledgments

The work reviewed in this paper was supported by the U.S. Air Force Office of Scientific Research, Defense Advanced Research Projects Agency, and Boeing. The authors express their thanks to G. Brown and L. Martinelli of Princeton University, D. Van Wie of Johns Hopkins University Applied Physics Laboratory, Yuri Raizer of Institute for Problems in Mechanics, Russian Academy of Sciences, L. Myrabo of Rensselaer Polytechnic Institute, and J. Silkey of Boeing for numerous valuable discussions, support, and advice.

References

[1] Oswatitsch, K., "Propulsion with Heating at Supersonic Speed," DLR, German Aerospace Research Center, Rept. 90, 1959.

[2] Investigation of Gas Flows with Heat Input in the Vicinity of the External Surface of a Flying Vehicle, Obzor BNTI TsAGI, (A Review by the Office of Scientific-and-Technical Information of Central Inst. of Aerohydrodynamics), No. 347, 1971.

[3] Reding, J. P., and Jesmen, D. M., "Effects of External Burning on Spike-Induced Separated Flow," *Journal of Spacecraft and Rockets*, Vol. 20, No. 3, 1983, pp. 452–453.

[4] Georgievskii, P. Yu., and Levin, V. A., *Supersonic Flow Past Volume Sources of Energy Release*, Mekhanika. Sovremen nye problemy (Mechanics: Modern Problems), Moscow State Univ., Moscow, 1987, pp. 93–97.

[5] Vlasov, V. V., Grudnitskii, V. G., and Rygalin, V. N., *Izvestiia Rossiiskoi Akademii Nauk Mekhanika Zhidkosti I Gaza*, Vol. 2, 1995, p. 142.

[6] Myrabo, L. N., Raizer, Yu. P., and Shneider, M. N., "Calculation and Similarity Theory of Experiment Simulating the Air-Spike Effect in Hypersonic Aerodynamics," *High Temperature*, Vol. 36, No. 2, 1998, pp. 287–292.

[7] Bushnell, D. M., "Supersonic Aircraft Drag Reduction," AIAA Paper 90-1596, June 1990.

[8] Levin, V. A., and Terent'eva, L. V., "Supersonic Flow over a Cone with Heat Release in the Neighborhood of the Apex," *Izvestiia Rossiiskoi Akademii Nauk Mekhanika Zhidkosti I Gaza*, Vol. 2, 1992, pp. 110–114.

[9] Georgievskii, P. Yu., and Levin, V. A., "Nonstationary Interaction of Sphere with Atmospheric-Temperature Heterogeneities in Supersonic-Flow," *Khimicheskaia Fizika*, Vol. 10, No. 12, 1993, pp. 1414–1423.

[10] Borzov, V. Yu., Rybka, I. V., and Yur'ev, A. S., "Power Deposition Estimation for Drag Reduction in Hypersonic Flow," *Inzhenerno Fizicheskii Zhurnal*, Vol. 63, No. 6, 1992, pp. 659–664.

[11] Riggins, D., Nelson, H. F., and Johnson, E., "Blunt-Body Wave Drag Reduction Using Focused Energy Deposition," *AIAA Journal*, Vol. 37, No. 4, 1999, pp. 460–467.

[12] Levin, V. A., Afonina, N. E., and Gromov, V. B., "Navier–Stokes Analysis of Supersonic Flow with Local Energy Deposition," AIAA Paper 99-4967, Nov. 1999.

[13] Takaki, R., and Liou, M.-S., "Parametric Study of Heat Release Preceding a Blunt Body in Hypersonic Flow," *AIAA Journal*, Vol. 40, No. 3, 2002, p. 501.

[14] Tretyakov, P., Garanin, A., Kraynev, V., Tupikin, A., and Yakovlev, V., *Proceedings of the 8th International Conference on Methods in Aerophysical Research, Novosibirsk: Izd. ITPM RAN*, Inst. of Theoretical and Applied Mechanics, Russian Academy of Science, Novosibirsk, Russia, 1996, p. 200.

[15] Knight, D., Kuchinskiy, V., Kuranov, A., and Sheikin, E., "Survey of Aerodynamic Flow Control at High Speed by Energy Deposition," AIAA Paper 2003-0525, Jan. 2003.

[16] Chernyi, G. G., "Some Recent Results in Aerodynamic Applications of Flows with Localized Energy Addition," AIAA Paper 1999-4819, Nov. 1999.

[17] Myrabo, L. N., and Raizer, Yu. P., "Laser-Induced Air Spike for Advanced Transatmospheric Vehicles," AIAA Paper 1994-2451, June 1994.

[18] Kandebo, S. W., "Air Spike Could Ease Hypersonic Flight Problems," *Aviation Week and Space Technology*, Vol. 142, No. 20, 1995, pp. 66–67.

[19] Myrabo, L. N.,Raizer, Y. P., Shneider, M. N., and Bracken, R., "Reduction of Drag and Energy Consumption During Energy Release Preceding a Blunt Body in Supersonic Flow," *High Temperature*, Vol. 42, No. 6, 2004, pp. 901–910. doi:10.1007/s10740-005-0035-2

[20] Myrabo, L. N., Raizer, Yu. P., and Shneider, M. N., "Drag and Total Power Reduction for Artificial Heat Input in Front of Hypersonic Blunt Bodies," *Third International Symposium on Beamed Energy Propulsion (ISBEP)*, American Inst. of Physics, Melville, NY, 2004, pp. 485–498.

[21] Chernyi, G. G., *Doklady Akademii Nauk SSSR*, Vol. 112, 1957, p. 213.

[22] Bracken, R. M., Myrabo, L. N., Nagamatsu, H. T., Meloney, E. D., and Shneider, M. N., "Experimental Investigation of an Electric Arc Air-Spike with and Without Blunt Body in Hypersonic Flow," AIAA Paper 2001-0796, Jan. 2001.
[23] Bracken, R. M., Myrabo, L. N., Nagamatsu, H. T., Meloney, E. D., and Shneider, M. N., "Experimental Investigation of an Electric Arc Air-Spike in Mach 10 Flow with Preliminary Drag Measurements," AIAA Paper 2001-2734, June 2001.
[24] Bracken, R. M., Hartley, C. S., Mann, G., Myrabo, L. N., Nagamatsu, H. T., Shneider, M. N., and Raizer, Y. P., "Experimental and Computational Parametric Drag Study of an "Air Spike" in Hypersonic Flow," AIAA Paper 2002-3784, July 2002.
[25] Kolesnichenko, Yu., Brovkin, V., Azarova, O., Grudnitsky, V., Lashkov, V., and Mashek, I., "Microwave Energy Release Regimes for Drag Reduction in Supersonic Flows," AIAA Paper 2002-0353, Jan. 2002.
[26] Kolesnichenko, Yu., Brovkin, V., Azarova, O., Grudnitsky, V., Lashkov, V., and Mashek, I., "MW Energy Deposition for Aerodynamic Application," AIAA Paper 2003-361, Jan. 2003.
[27] Georgievsky P. Yu., and Levin, V. A., "Bow-Shock-Wave-Structure Dynamics for Pulse-Periodic Energy Input into a Supersonic Flow," *5th International Workshop on Magneto-Plasma Aerodynamics for Aerospace Applications*, Moscow, 2003, pp. 228–233.
[28] Curran, E. T., and Murthy, S. N. B. (eds.), *Scramjet Propulsion*, Vol. 189, Progress in Astronautics and Aeronautics, AIAA, Reston, VA, 2000.
[29] Van Wie, D. M., "Scramjet Inlets," *Scramjet Propulsion*, edited by E. T. Curran, and S. N. B. Murthy, Vol. 189, Progress in Astronautics and Aeronautics, AIAA, Reston, VA, 2000, Chap. 7, pp. 447–511.
[30] Shneider, M. N., Macheret, S. O., Miles, R. B., and Van Wie, D. M., "MHD Power Generation in Scramjet Engines in Conjunction with Inlet Control," AIAA Paper 2004-1197, Jan. 2004.
[31] Shneider, M. N., and Macheret, S. O., " Modeling of Plasma Virtual Shape Control of Ram/Scramjet Inlet and Isolator," AIAA Paper 2004-2662, June 2004; also *Journal of Propulsion and Power*, Vol. 22, No. 2, 2006, pp. 447–454.
doi:10.2514/1.16959
[32] Shneider, M. N., and Macheret, S. O., "Modeling Plasma and MHD Effects in Hypersonic Propulsion Flowpath," AIAA Paper 2005-5051, June 2005.
[33] Macheret, S. O., Shneider, M. N., and Miles, R. B., "Optimum Performance of Electron Beam Driven MHD Generators for Scramjet Inlet Control," AIAA Paper 2003-3763, June 2003.
[34] Shneider, M. N., Macheret, S. O., and Miles, R. B., "Nonequilibrium Magnetohydrodynamic Control of Scramjet Inlets," AIAA Paper 2002-2251, May 2002.
[35] Shneider, M. N., Macheret, S. O., and Miles, R. B., "Comparative Analysis of MHD and Plasma Methods of Scramjet Inlet Control," AIAA Paper 2003-0170, Jan. 2003.
[36] Kuranov, A. L., and Sheikin, E. G., "MHD Control on Hypersonic Aircraft Under AJAX Concept: Possibilities of MHD Generator," AIAA Paper 2002-0490, Jan. 2002.
[37] Macheret, S. O., Shneider, M. N., and Miles, R. B., "External Supersonic Flow and Scramjet Inlet Control by MHD with Electron Beam Ionization," AIAA Paper 2001-0492, Jan. 2001.
[38] Macheret, S. O., Shneider, M. N., and Miles, R. B., "Magnetohydrodynamic Control of Hypersonic Flow and Scramjet Inlets Using Electron Beam Ionization," *AIAA Journal*, Vol. 40, No. 1, 2002, pp. 74–81.
[39] Macheret, S. O., Shneider, M. N., and Miles, R. B., "Magnetohydrodynamic and Electrohydrodynamic Control of Hypersonic Flows of Weakly Ionized Plasmas," AIAA Paper 2002-2249, May 2002.
[40] Macheret, S. O., Shneider, M. N., Miles, R. B., Lipinski, R. J., and Nelson, G. L., "MHD Acceleration of Supersonic Air Flows Using Electron Beam-Enhanced Conductivity," AIAA Paper 98-2922, June 1998.
[41] Macheret, S. O., Shneider, M. N., and Miles, R. B., "Electron Beam Generated Plasmas in Hypersonic MHD Channels," AIAA Paper 99-3635, June 1999.
[42] Macheret, S. O., Shneider, M. N., and Miles, R. B., "MHD Power Extraction from Cold Hypersonic Air Flow with External Ionizers," AIAA Paper 99-4800, Nov. 1999; also *Journal of Propulsion and Power*, Vol. 18, No. 2, 2002, pp. 424–431.
[43] Macheret, S. O., Shneider, M. N., Miles, R. B., and Lipinski, R. J., "Electron Beam Generated Plasmas in Hypersonic Magnetohydrodynamic Channels," *AIAA Journal*, Vol. 39, No. 6, 2001, pp. 1127–1136.
[44] Macheret, S. O., Shneider, M. N., and Miles, R. B., "Optimum Performance of Electron Beam Driven Magnetohydrodynamic Generators for Scramjet Inlet Control," *AIAA Journal*, Vol. 45, No. 9, 2007, pp. 2157–2163.
doi:10.2514/1.16955
[45] Macheret, S. O., Shneider, M. N., and Miles, R. B., "Nonequilibrium Magnetohydrodynamic Control of Scramjet Inlets," AIAA Paper 2002-2251, May 2002.
[46] Macheret, S. O., Shneider, M. N., and Miles, R. B., "Scramjet Inlet Control by Off-Body Energy Addition: A Virtual Cowl," AIAA Paper 2003-0032, Jan. 2003; also *AIAA Journal*, Vol. 42, No. 11, 2004, pp. 2294–2302.
[47] Kuranov, A. L., and Sheikin, E. G., "MHD Control by External and Internal Flows in Scramjet Under "AJAX" Concept," AIAA Paper 2003-173, Jan. 2003.
[48] Leonov, S., Bityurin, V., Youriev, A., Savishchenko, N., Pirogov, S., and Ryzhov, E., "Problems in Energetic Method in Drag Reduction and Flow/Flight Control," AIAA Paper 2003-0035, Jan. 2003.
[49] ASTRA, *Computer Program for Calculation of Thermodynamic Properties of Individual Substances and Mixtures*, edited by B. G. Trusov, Bauman Technical Univ., Moscow, April 1991.
[50] Girgis, I. G., Shneider, M., Macheret, S., Brown, G., and Miles, R. B., "Creation of Steering Moments in Supersonic Flow by Off-Axis Plasma Heat Addition," AIAA Paper 2002-0129, Jan. 2002; also *Journal of Spacecraft and Rockets*, Vol. 43, No. 3, 2006, pp. 607–613.
[51] McAndrew, B., "Aerodynamic Control in Compressible Flow Using Microwave Driven Discharges," Ph.D. Dissertation, Princeton Univ., Princeton, NJ, 2003.
[52] McAndrew, B., Kline, J., and Miles, R. B., "Development of a Supersonic Plasma Wind Tunnel," AIAA Paper 2003-0033, Jan. 2003.
[53] Seebass, R., "Sonic Boom Theory," *Journal of Aircraft*, Vol. 6, No. 3, 1969, pp. 177–184.
[54] McLean, F. E., "Configuration Design for Specific Pressure Signature Characteristics," *Sonic Boom Research*, edited by I. R. Schwartz, NASA SP-180, 1968, pp. 37–40.
[55] Cheng, Sin-I, U.S. Patent 3737119, filed 15 June 1970, issued 5 June 1973.
[56] Crow, S. C., and Bergmeier, G. G., "Active Sonic Boom Control," *Journal of Fluid Mechanics*, Vol. 325, Oct. 1996, pp. 1–28.
[57] Miles, R. B., Martinelli, L., Macheret, S. O., Shneider, M. N., Girgis, I. G., Zaidi, S. H., and Mansfield, D. K., "Suppression of Sonic Boom by Dynamic Off-Body Energy Addition and Shape Optimization," AIAA Paper 2002-0150, Jan. 2002.
[58] Yan, H., Adelgren, R., Elliott G., Knight, D., Beuthner, T., and. Ivanov, M., "Laser Energy Deposition in Intersecting Shocks," AIAA Paper 2002-2729, June 2002.
[59] Kandala, R., and Candler, G., "Numerical Studies of Laser-Induced Energy Deposition for Supersonic Flow Control," AIAA Paper 2003-1052, Jan. 2003.
[60] Zaidi, S. H., Shneider, M. N., Mansfield, D. K., Ionikh, Yu. Z., and Miles, R. B., "Influence of Upstream Pulsed Energy Deposition on a Shockwave Structure in Supersonic Flow," AIAA Paper 2002-2703, June 2002.
[61] Zaidi, S. H., Shneider, M. N., and Miles, R. B., "Investigation of Shock-Wave Mitigation Through an Off-Body Pulsed Energy Deposition," *AIAA Journal*, Vol. 42, No. 2, 2004, pp. 326–331.
doi:10.2514/1.9097

S. Macheret
Guest Editor